Optimal Solar Sail Interplanetary Heteroclinic Transfers for Novel Space Applications

G. Mingotti* and J. Heiligers† and C. McInnes‡

University of Strathclyde, Glasgow, G1 1XJ, United Kingdom

This paper investigates the design and optimization of solar sail interplanetary trajectories connecting both Libration Point Orbits (LPOs) and Distant Periodic Orbits (DPOs) belonging to different restricted three-body problems: namely the Sun–Earth model and the Sun–Venus one. Assuming the Sun always as first primary, the Earth and Venus are the second primary, and their relative models are coupled together with the view of defining heteroclinic connections. On suitable Poincaré sections, solar sail sets are constructed to obtain transit conditions from LPOs of the departure dynamical system to either LPOs or DPOs of the arrival one. Starting from initial guesses that assume a constant attitude of the solar sail, an optimal control problem is formulated, encompassing a trade-off between minimum transfer time and minimum solar sail steering effort, and it is solved with a direct pseudospectral method. At the optimization stage, variable attitude solar sails are investigated, assuming spacecraft with different control capabilities.

Nomenclature

LPO	Libration Point Orbit
PL	Planar Lyapunov Orbit

*Research Associate, Advanced Space Concepts Laboratory, Department of Mechanical & Aerospace Engineering; e-mail: giorgio.mingotti@strath.ac.uk

†Research Associate, Advanced Space Concepts Laboratory, Department of Mechanical & Aerospace Engineering; e-mail: jeannette.heiligers@strath.ac.uk

‡Professor, Advanced Space Concepts Laboratory, Department of Mechanical & Aerospace Engineering; e-mail: colin.mcinnes@strath.ac.uk

NH	Northern Halo Orbit
VL	Vertical Lyapunov Orbit
DPO	Distant Periodic Orbit

I. Introduction

Research in the field of solar sailing is flourishing, sparked by successes such as JAXA's IKAROS[1] mission and new solar sail initiatives including NASA's Sunjammer mission.[2] Its potential lies in the fact that solar sail missions are not constrained by a propellant mass: by using the Sun as "propellant source", solar sails obtain their propulsive acceleration by reflecting photons off a highly reflective membrane. This gives solar sails a theoretically unlimited lifetime and enables a wealth of novel orbits and space applications, including periodic orbits around sail displaced libration points. Moreover, with the increase of the area-to-mass ratio, solar radiation pressure has a significant effect on the interplanetary transfer design process. Previous applications of solar sails have already been designed assuming the two-body problem, i.e. McInnes,[3] and the three-body problem, i.e. Baoyin.[4]

It is well-known that the three-body system generates five natural libration points, around which periodic orbits can be found (LPOs). By adding a solar sail to the dynamical model, the collinear Lagrange points as well as the periodic orbits around them are displaced Sunward along the Sun-sail line. Therefore, natural L_1-and L_2-orbits will therefore shift away and towards the secondary body, respectively, allowing for additional interesting science. Firstly, the aim of this paper is to describe the first-guess generation process - based on a few design variables - of solar sail trajectories for the Earth-to-Venus applicative scenario. Both the connections of an Earth L_1 planar Lyapnunov orbit with a Venus DPO, and of an Earth L_1 northern Halo with a Venus L_2 vertical Lyapunov are investigated, thereby building on the concept named "patched restricted three-body problems approximation".[5] In this approach, intersections in configuration space of the invariant manifolds of the two restricted three-body problems are searched for. For example, the unstable manifold of a L_1 northern Halo in the Sun–Earth problem is considered as well as the stable manifold of a L_2 vertical Lyapunov orbit in the Sun–Venus problem. If these intersect, an Earth–Venus low-energy transfer with at most one deep-space manoeuvre exists. Unfortunately, no intersection exists among ballistic manifolds of inner planets.[6] Therefore, initial guesses for these transfers are designed exploiting the solar sail acceleration and the intrinsic dynamics of the three-body systems involved, assuming a constant attitude of the sail with respect to the Sun-sail line.

Special*dedicated sets* are then introduced to exploit the combined use of solar radiation pressure with invariant manifold trajectories, aiming at defining feasible first guess solutions.

This approach enables a radically new class of missions, whose solutions are not obtainable neither through the patched-conics method nor through the classic invariant manifolds technique. The key idea is to replace invariant manifolds with *solar sail sets*, and to manipulate the latter in the same way the manifolds are used to design space transfers.[7,8] By including a solar sail acceleration and fixing the attitude of the solar sail with respect to the Sun-sail line, intersections between restricted three-body models can be found on suitable Poincaré sections, also for the inner planets. Alongside the exploitation of the n-body problems' intrinsic dynamics, the propellant-free feature of solar sails is used in order to define efficient trajectories.

Then, the initial guesses reveal to be sub-optimal in the sense that minor discontinuities in position and velocities at the transit point between the two three-body systems need to be overcome. This is achieved by transferring the first-guess trajectories to a direct pseudospectral method, relieving the constraint on the constant attitude. Then the accompanying optimal control problems are solved.

The objective function of the optimal control problem the time of flight. The latter objective ensures that the trajectories can be performed with low control authority solar sails, while more emphasis can be put on the first objective for high control authority solar sails. As such, applications of the found trajectories cover the entire spectrum of sail length-scales: distributing micro-sized, low control authority solar sails along a trajectory connecting an Earth L_1-orbit with an L_2-orbit at Venus establishes a continuous Earth–Venus communication link, even during Venusian occultation; alternatively, a meso-sized, fully steerable solar sail can enable an interesting planetary observation platform at Venus; and finally, in the macro-scale, the previously mentioned Earth–Venus link allows a vital gateway for cargo transport for future human exploration on Venus.

The paper is organized as follows. In section II some background notions on the circular restricted three-body problem, its periodic orbits and invariant manifold structure are given. Then, section III introduces solar radiation pressure into the restricted three-body problem and defines the special dedicated sets. In section IV the first guess design technique is formulated: the solar sail interplanetary heteroclinic connections are generated. The optimal control problem is then discussed in sections V and VI, while the optimal heteroclinic transfer connections a represented in section VII. Finally, conclusive remarks are given in VIII.

II. Dynamical Models

In this section, the dynamical system investigated in this work is described, i.e. the three-dimensional Circular Restricted Three-Body Problem (CRTBP), with its periodic orbits and invariant manifold structure. The dynamics described in the following holds for the Sun–

Earth (SE) and the Sun–Venus (SV) problem, respectively.

A. The Three-Dimensional Circular Restricted Three-Body Problem

The motion of the spacecraft, P_3, of mass m_3, is studied in the gravitational field generated by two primaries, P_1, P_2, of masses m_1, m_2, respectively, assumed to move in circular motion about their common center of mass (see Fig. 1(a)). It is assumed that P_3 moves under the non-dimensional equations[9]

$$\ddot{x} - 2\dot{y} = \frac{\partial \Omega_T}{\partial x}, \qquad \ddot{y} + 2\dot{x} = \frac{\partial \Omega_T}{\partial y}, \qquad \ddot{z} = \frac{\partial \Omega_T}{\partial z}, \tag{1}$$

where the auxiliary function is

$$\Omega_T(x, y, z, \mu) = \frac{1}{2}(x^2 + y^2) + \frac{1-\mu}{r_1} + \frac{\mu}{r_2} + \frac{1}{2}\mu(1-\mu), \tag{2}$$

and $\mu = m_2/(m_1 + m_2)$ is the mass parameter of the three-body problem. Eqs. (1) are written in a barycentric rotating frame with non-dimensional units: the angular velocity of P_1, P_2, their distance, and the sum of their masses are all set to the unit value. Thus, P_1, P_2 have scaled masses $1 - \mu$, μ, and are located at $(-\mu, 0)$, $(1 - \mu, 0)$, respectively. The distances in Eq. (2) are therefore

$$r_1^2 = (x + \mu)^2 + y^2 + z^2, \qquad r_2^2 = (x + \mu - 1)^2 + y^2 + z^2. \tag{3}$$

As unit of length, λ, the distance between the primaries is selected, and $1/\omega$ is chosen as unit of time, τ, yielding $\omega = 1$, and so one orbital period of the planet around the Sun is represented by 2π.

For fixed μ, the energy of P_3 is represented by the Jacobi integral which reads

$$\mathcal{J}(x, y, z, \dot{x}, \dot{y}, \dot{z}, \mu) = 2\Omega_T(x, y, z, \mu) - (\dot{x}^2 + \dot{y}^2 + \dot{z}^2), \tag{4}$$

and, for a given energy $\mathcal{C}$, it defines a three-dimensional manifold

$$\mathcal{M}(\mathcal{C}) = \{(x, y, z, \dot{x}, \dot{y}, \dot{z}, \mu) \in \mathbb{R}^6 \,|\, \mathcal{J}(x, y, z, \dot{x}, \dot{y}, \dot{z}, \mu) - \mathcal{C} = 0\}. \tag{5}$$

The projection of $\mathcal{M}$ on the configuration space (x, y) defines the Hill's curves bounding the allowed and forbidden regions of motion associated with prescribed values of $\mathcal{C}$. The aforementioned three-dimensional manifold of the states of motion has singular points which are also equilibrium points for the dynamical system. The CRTBP is used to model the

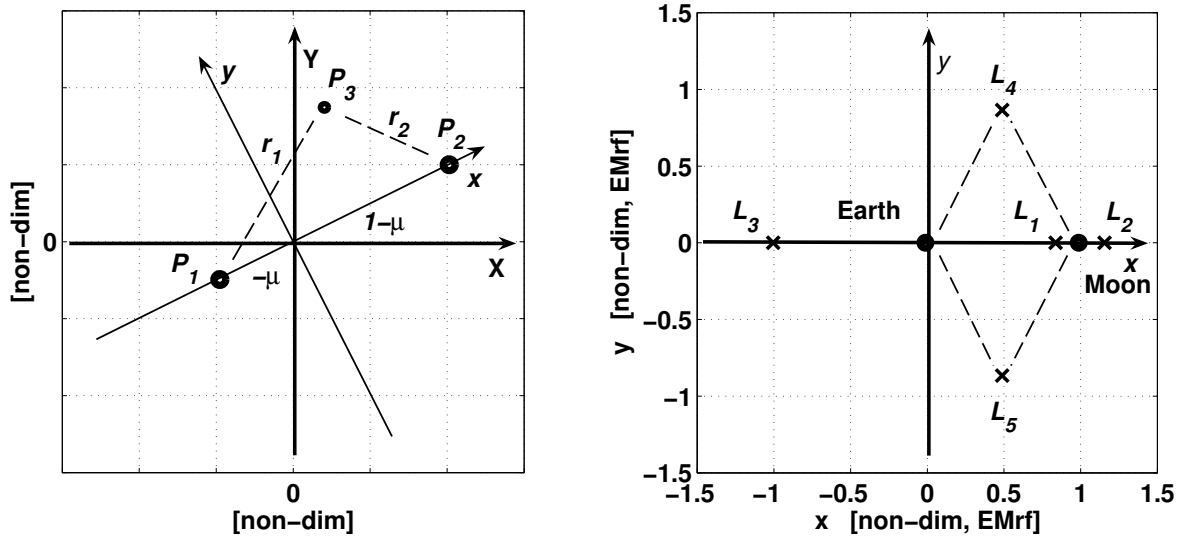

(a) Circular restricted three-body problem.

(b) Libration point location.

Figure 1. Circular restricted three-body problem geometry and libration point location.

third body motion in the Sun–Earth system, whose mass parameter is $\mu = 3.003460 \times 10^{-6}$ (therefore not including the Moon mass), and in the Sun–Venus system, whose mass parameter is $\mu = 2.447131 \times 10^{-6}$.[9]

The CRTBP has five well-known equilibrium points, L_j, whose energy is $\mathcal{C}j$, $j = 1, \ldots, 5$. They are classified as *collinear* (L_1, L_2, L_3), which belong to the x-axis of the rotating reference system, and as *equilateral* (see Fig. 1(b)). The latter form two equilateral triangles, symmetric with respect to the x-axis, with the two primaries as vertexes.[10–12]

B. Libration Point Periodic Orbits

Concerning the CRTBP, around the three collinear equilibrium points and associated with their center-like behavior, there are periodic and quasi-periodic orbits. Recalling the conservative property of Hamiltonian systems, periodic orbits can be grouped in families and they are function of just one scalar: the amplitude $\hat{A}$ of the orbit. In detail, the orbits related to the linear oscillators of the linearized problem belong to the Lyapunov family, planar and vertical.

There is an analytic solution of the latter, associated with the linearized problem and thus characterized by infinitesimal dimensions. Space mission design usually involves Lyapunov orbits with prescribed wider amplitude and governed by the complete dynamics of the problem. The computation of these orbits is obtained through a numerical approach, based on *perturbation* techniques, in order to correct the analytic initial estimates, and on *continuation* techniques, in order to expand the infinitesimal orbits. Other interesting solutions are the two-dimensional tori, associated with the Lissajous orbits arising from the

Table 1. Departure and arrival LPOs and DPOs for the Earth-to-Venus applicative scenarios. NH stands for northern Halo orbit, PL for planar Lyapunov orbit, VL for vertical Lyapunov orbit and DP for Distant Periodic orbit. A_z is the out-of-plane amplitude, $\mathcal{C}$ is the Jacobi constant and P_O is the period of the selected departure and arrival orbits.

Departure Orbit	$\hat{A}$ [km]	$\mathcal{C}$ [−, SErf]	P_O [−, SErf]	Arrival Orbit	$\hat{A}$ [km]	$\mathcal{C}$ [−, SVrf]	P_O [−, SVrf]
Earth PL-L1	650×10^3	3.0006874	3.1860	Venus DPO	–	3.0003567	4.1830
Earth NH-L1	650×10^3	3.0006874	3.0388	Venus VL-L2	–	3.0001037	4.1932

product of the two linear oscillators.

It is well known from theory, that if the phase space of a dynamical system changes substantially varying the value of a certain parameter, this behavior is known as *bifurcation* phenomenon. In the CRTBP framework, the planar Lyapunov orbits defined with the amplitude $\hat{A}$ as unique parameter, according to the bifurcation effect, give origin to a family of three-dimensional orbits with a different period and with a modified relative invariant manifold structure.

Moreover, once the *out-of-plane* A_z amplitude overcomes a limit value $\bar{A}_z$, the frequency of the *in-plane* oscillatory motion achieves the value of the frequency of the one out of the plane, and three-dimensional halo orbits emerge.[13] The lack of an analytic solution in the CRTBP, the significant nonlinearity of the problem as well as the strong dependence on variations of initial conditions, imply that the determination of such orbits is not trivial: their computation is possible starting from a semi-analytic formulation, according to the systematic approach proposed by Richardson,[14,15] and then following approximations based on differential corrections.

In this paper, two different types of libration point orbits are investigated: three-dimensional (x, z)-plane symmetric northern Halo (with the maximum out-of-plane displacement $z > 0$) and three-dimensional (x, z)-plane symmetric southern Halo (with the maximum out-of-plane displacement $z < 0$).

In this work, four different classes of libration point orbits are investigated: (x, z)-plane symmetric Planar Lyapunov, (x, z)-plane, (x, y)-plane and x-axis symmetric eight-shaped Vertical Lyapunov,[16] (x, z)-plane symmetric Northern Halo (with the maximum out-of-plane displacement $z > 0$) and (x, z)-plane symmetric Southern Halo (with the maximum out-of-plane displacement $z < 0$).

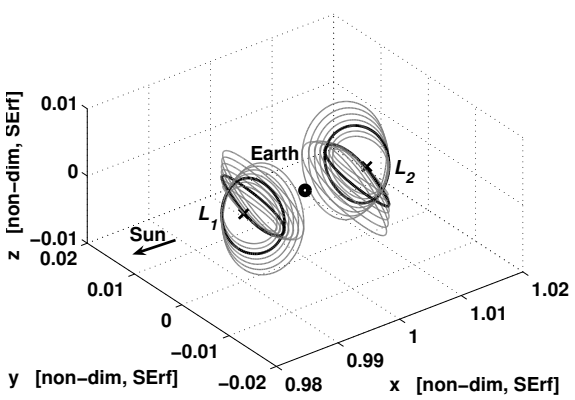

(a) Family of SE halo periodic orbits. The bold lines stand for the selected ones (see Tab. 1).

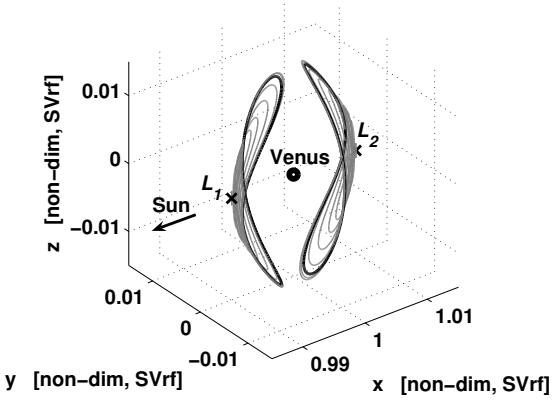

(b) Family of SV vertical Lyapunov orbits. The bold lines stand for the selected ones (see Tab. 1).

Figure 2. Sample of periodic orbits in the Sun–Earth and Sun–Venus restricted three-body problems.

C. Distant Prograde Periodic Orbits

According to the classic formulation of the CRTBP, μ represents the mass parameter of the problem. When its value is very close to zero, i.e. the mass of the small primary tends to vanish, most of the practical applications of restricted problems are covered. Therefore, particular periodic orbits arise and their stability properties are investigated. At first view it seems to be trivial: the third body is subjected to the attraction of the first body only, so that its motion is given by the formulas of the two-body problem. However, first Hill, later Kevorkian and Szebehely, showed that a nontrivial problem can be obtained in the following way. Let μ be small, but not zero. In the vicinity of the second body, there is then a small region where the effect of the smaller primary is not negligible, but rather of the same or larger order than the contribution of the main primary. Assuming $\mu \to 0$ and enlarging the vicinity of the second body, after an appropriate change of scale and origin, the limit process gives evidence of a nontrivial problem and of orbits that are not those of the two-body problem. Through this new model, known as Hill's problem, the motion in the neighborhood of the smaller primary is described and investigated.

In this framework, recalling $\mu \to 0$), there exist periodic orbits. Due to the existence of the integral of motion, these orbits are grouped in one-parameter families, each family containing a simple infinity of periodic orbits, whose properties vary continuously from one end of the family to the other. For non-zero mass parameters, a transformation is needed to obtain these orbits in the CRTBP from those available in literature.[17]

Theory predicts, however, that there are infinitely many families of periodic orbits. The simplest of them are those symmetric with respect to the x-axis, and *simple-periodic*; i.e., intersecting the x-axis only twice. According to Hénon nomenclature,[17] there are five groups.

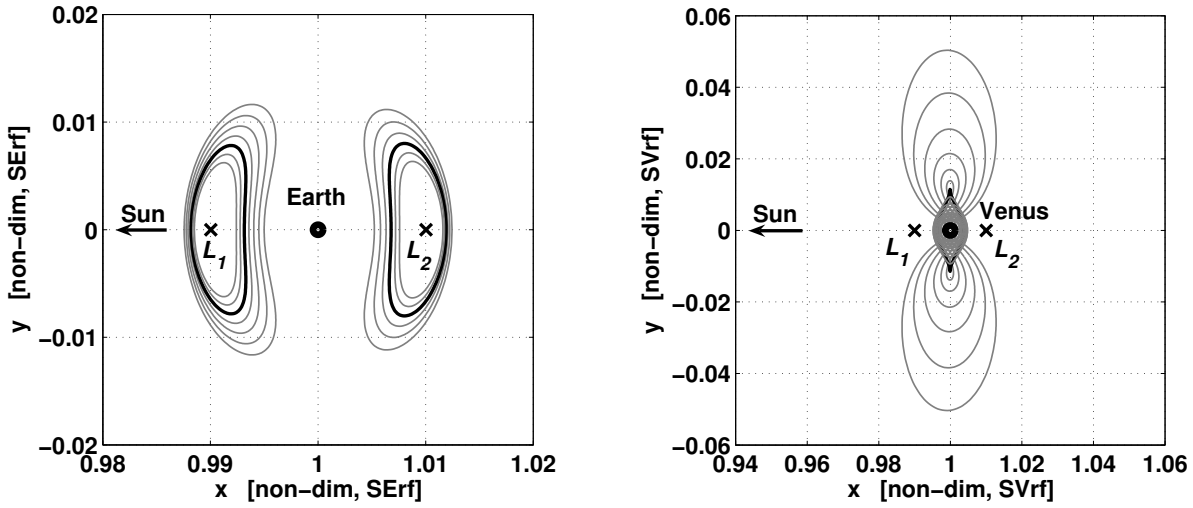

(a) Family of SE planar Lyapunov periodic orbits. The bold lines stand for the selected ones (see Tab. 1).

(b) Family of SV distant prograde periodic orbits. The bold lines stand for the selected ones (see Tab. 1).

Figure 3. Sample of periodic orbits in the Sun–Earth and Sun-Venus restricted three-body probles.

Orbits of families a and c originating as libration point orbits, are all unstable. Orbits of family f, originating as retrograde orbits about the smaller primary, are all stable. Orbits of families g and g', originating as orbits only around the smaller primary, are stable below a certain energy level and unstable above that value. These orbits are computed numerically from the initial conditions in Ref. 17. A numerical continuation procedure, implementing μ as continuation parameter, together with a simple shooting algorithm, delivers DPOs in the Sun–Venus CRTBP with enough accuracy, in the same way as in Ref. 18 for the Earth–Moon system. More specifically, a subset of the g-type orbits is considered in this paper for which $\Gamma < 4.99986$ and the stability index is greater than one. As the g-orbits originate from the central orbits around the smaller primary, they are stable in the region close to the smaller primary, though their stability index continuously varies when Γ decreases (and the orbit's size increases accordingly). In particular, for $\Gamma < 4.99986$ the g-orbits become unstable. Since this condition is reached when portions of the orbits lie far from the smaller primary (farther than the two libration points close to it), these orbits are also known as distant prograde periodic orbits.

D. Invariant Manifold Structure

In the CRTBP framework, a set can be said to be invariant if any orbit that originates from itself is bounded within limits during the time evolution of the dynamics: namely, an invariant manifold can be viewed as a combination of orbits that form a surface. In

detail, equilibrium points, periodic orbits as well as the Jacobi integral expressed in Eq. (4), all represent invariant manifolds, zero-dimensional, one-dimensional and five-dimensional, respectively. The motion that starts from any of those manifolds is bounded in the same subspace of its origin, under the flow of the dynamical system. From the perspective of space mission analysis, one-dimensional stable and unstable manifolds V_{L_j} related to the fixed points, as well as the two-dimensional ones W_{L_j} associated with the periodic orbits around the same points, for $j = 1, 2$, are of great interest.

Invariant manifolds associated with LPOs are appealing for space mission design (see Fig. 4). They are classified in stable $W^s_{L_j}$, for $j = 1, 2$, if the third body - from an initial condition belonging to the surface itself - asymptotically moves to the periodic orbit; moreover, if a spacecraft from an initial condition on $W^u_{L_j}$, for $j = 1, 2$, moves indefinitely away from a periodic orbit, that manifold is said to be unstable. Such surfaces in the configuration space have a *tube*-like structure and they play a role of *separatrices*[19] of the motion: trajectories inside these subspaces are transit orbits that allow the third body to move from one primary to the other, while those outside these subspaces are non-transit orbits.

As far as it concerns the CRTBP, in order to investigate the hyperbolic-like behavior of periodic orbits around libration points, the classic approach is based on the Floquet theory that studies the linear approximation of the flow mapping around a periodic orbit.[20] Thus, once the state transition matrix associated with a periodic orbit is obtained, the *monodromy* matrix $\mathbf{M}$, the manifolds are computed by propagating the flow along the directions corresponding to the Floquet multipliers of that orbit. In particular, if $\mathbf{y}$ is a point belonging to the periodic orbit, the monodromy matrix represents the first-order approximation for the mapping of a point $\mathbf{y}_k$, considered in a small neighborhood, through

$$\mathbf{y} \mapsto \mathbf{y}_k + \mathbf{M}(\mathbf{y} - \mathbf{y}_k). \tag{6}$$

In detail, it is possible to construct the two-dimensional stable manifold $W^s_{L_j}$, for $j = 1, 2$, as the connection of all the one-dimensional stable manifolds associated with each q point of the periodic orbit, named $\mathbf{y}^q$

$$\mathbf{y}^q_{k,s} = \mathbf{y}^q \pm \varepsilon \mathbf{v}^q_s. \tag{7}$$

In the same way, the two-dimensional unstable manifold $W^u_{L_j}$, for $j = 1, 2$, is formulated as

$$\mathbf{y}^q_{k,u} = \mathbf{y}^q \pm \varepsilon \mathbf{v}^q_u, \tag{8}$$

where $\varepsilon = 1.0 \times 10^{-6}$ is a scalar parameter that represents the *magnitude* of the shift along the stable $\mathbf{v}^q_s$ and unstable $\mathbf{v}^q_u$ normalized eigenvector of the monodromy matrix $\mathbf{M}$ evaluated at the fixed point $\mathbf{y}^q$, respectively.[21]

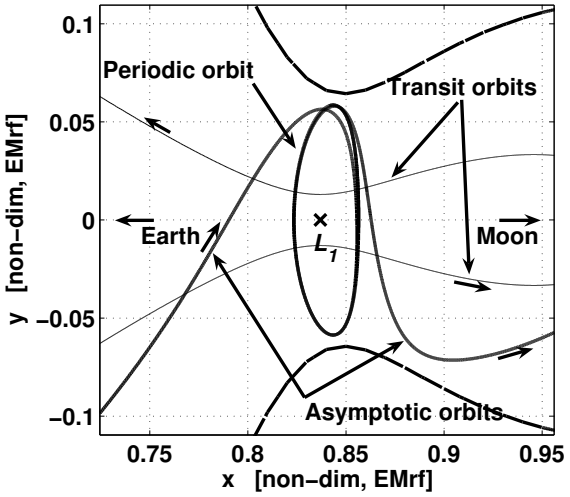

(a) Orbital motion around the libration point L_1 in the Earth–Moon system.

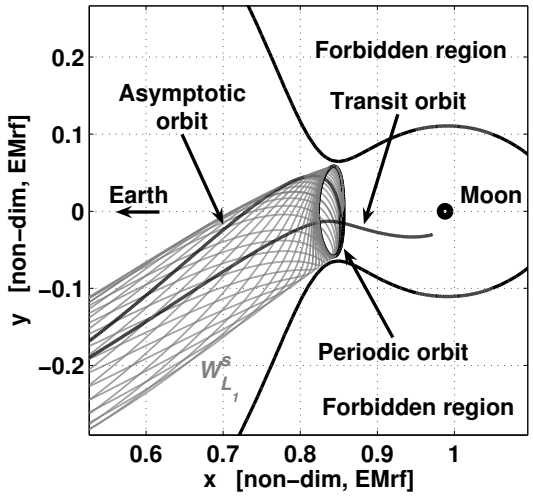

(b) Invariant manifold structure associated to a LPO around L_1 in the Earth–Moon system.

Figure 4. Orbital motion and invariant manifold structure around the libration point L_1.

The symbol $\pm$ denotes the existence of two branches for each manifold. Considering the fixed point L_1 of Sun–Earth system, the branch associated with the symbol $-$ is the branch of the manifold originating from the L_1-region and moving, internally, in the direction of the Sun ($W^{s,I}_{L_1}$, $W^{u,I}_{L_1}$). On the other hand, the branch of the manifold related to the symbol $+$ is the one departing from the L_2-region and moving, externally, away from the Earth ($W^{s,E}_{L_2}$, $W^{u,E}_{L_2}$).

Finally, it is possible to flow the previous initial conditions, obtained through the linear analysis, under the complete nonlinear differential system of Eqs. (1). This is valid thanks to the property that the stable and unstable manifolds associated with periodic orbits are locally tangent at the origin to the subspace of the eigenvectors of the monodromy matrix.[9–11]

The orbits belonging to the Lyapunov family, to the halo family as well as to the unstable DPO g-family, show an interesting behavior as they possess local stable and unstable manifolds that can be globally extended. The structure of these manifolds define subsets that may provide free transport channels for a massless particle (i.e. a rock or a spacecraft). From a mission design point of view, a spacecraft can travel naturally to or from unstable periodic orbits respectively along their stable or unstable manifolds, respectively, by only introducing small perturbation maneuvers.[22] This complex transfer structure, in terms of both stable and unstable manifold, intersect many interesting regions in the restricted three-body system: the small primary neighborhood and the libration point vicinity.

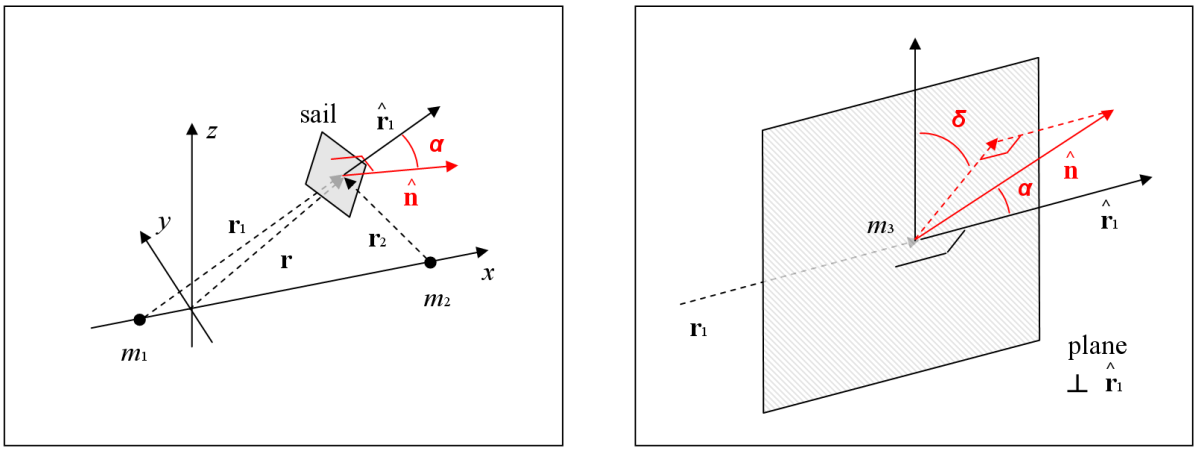

(a) Solar sail geometry: the cone angle α.

(b) Solar sail geometry: the clock angle δ.

Figure 5. Solar sail geometry in the circular restricted three-body problem: the cone angle α and the clock angle δ.

III. Solar Radiation Pressure and Dedicated Sets

In this section, the perturbed circular restricted three-body problem by a prescribed control law and special *dedicated sets* are introduced. As a direct consequence, the *solar sail sets* associated to the departure and arrival periodic orbits are described. The formulation holds for the Sun–Earth and the Sun–Venus system, respectively.

A. The Perturbed, Three-Dimensional Circular Restricted Three-Body Problem

To model the motion of a massless particle P_3 under both the gravitational attractions of P_1, P_2, and solar radiation pressure, the perturbed CRTBP is introduced:[23]

$$\ddot{x} - 2\dot{y} = \frac{\partial \Omega_T}{\partial x} + a_s s_x, \qquad \ddot{y} + 2\dot{x} = \frac{\partial \Omega_T}{\partial y} + a_s s_y, \qquad \ddot{z} = \frac{\partial \Omega_T}{\partial z} + a_s s_z, \tag{9}$$

where $\hat{\mathbf{s}} = (s_x, s_y, s_z)^\top$ is the normalized acceleration direction due to the effect of solar radiation pressure on the sail surface and, considering an ideal sail, it is aligned with its normal component $\hat{\mathbf{n}}$, i.e. $\hat{\mathbf{s}} \equiv \hat{\mathbf{n}}$. The magnitude of this acceleration is

$$a_s = \beta \frac{1-\mu}{r_1^2} (\hat{\mathbf{s}} \cdot \hat{\mathbf{r}}_1)^2, \tag{10}$$

where β is the lightness number of the sail and $\mathbf{r}_1 = (x+\mu, y, z)^\top$ is the Sun-sail line vector. Moreover, the angle $\alpha = \cos^{-1}(\hat{\mathbf{s}} \cdot \hat{\mathbf{r}}_1)$ is known as the *cone angle* (see Fig. 5(a)).

Assuming that the attitude of the sail is controllable, solar radiation pressure rather than

a passive perturbation becomes a way to control the orbital dynamics of the spacecraft. In addition to the cone angle, another angle is introduced to univocally define the attitude of the solar sail: the *clock angle* δ (see Fig. 5(b)), that is the angle measured clockwise around $\hat{\mathbf{r}}_1$, starting from the vertical plane, of the component of $\hat{\mathbf{n}}$ perpendicular to $\hat{\mathbf{r}}_1$ (recalling that for an ideal sail $\hat{\mathbf{s}} \equiv \hat{\mathbf{n}}$). In order to build first guess solutions, the control direction $\hat{\mathbf{s}}(t) = (s_x(t), s_y(t), s_z(t))^\top$, with $t \in [t_i, t_f]$, in Eqs. (9) is a-priori imposed, giving, at this stage, to the control law $\mathbf{R}(\alpha, \delta) = a_s \hat{\mathbf{s}}(t)$ a prescribed shape. In detail, the profile over time of the cone angle $\alpha(t)$ and the clock angle $\delta(t)$ is assigned. Dedicated solar sail sets can be defined under this assumption.

B. Definition of Solar Sail Dedicated Sets

Let $\mathbf{y}_i$ be a vector representing a generic initial state, $\mathbf{y}_i = (x_i, y_i, z_i, \dot{x}_i, \dot{y}_i, \dot{z}_i)$; then let the flow of system of Eqs. (9) be $\phi_{\mathbf{R}(\alpha,\delta)}(\mathbf{y}_i, t_i; t)$ at time t starting from $(\mathbf{y}_i, t_i)$ and considering the control law, based on the exploitation of solar radiation pressure, $\mathbf{R}(\alpha, \delta) = a_s \hat{\mathbf{s}}(t)$, $t \in [t_i, t_f]$.

With this notation, it is possible to define the generic point of a solar sail trajectory through

$$\mathbf{y}(t) = \phi_{\overline{\mathbf{R}}(\alpha,\delta)}(\mathbf{y}_i, t_i; t), \tag{11}$$

where $\overline{\mathbf{R}}(\alpha, \delta)$ is the control vector assuming solar sail with fixed attitude with respect to the Sun-sail line, i.e. with constant cone angle α and constant clock angle δ. Solar sail acceleration magnitude is then computed via Eq. (10).

Let $Q(\theta)$ be a surfaces of section perpendicular to the (x, y)-plane that forms an angle θ with the x-axis.

The solar sail orbit, for a chosen value of ϵ, is

$$\gamma_{\overline{\mathbf{R}}(\alpha,\delta)}(\mathbf{y}_i, \tau, \theta) = \left\{ \phi_{\overline{\mathbf{R}}(\alpha,\delta)}(\mathbf{y}_i, t_i; \tau) \,|\, 0 \le \tau \le t_Q \right\}, \tag{12}$$

where the dependence on the initial state $\mathbf{y}_i$ is kept. In Eq. (12), τ is the duration of the solar sail contribution, whereas t_Q is the time at which the orbit intersects (for the first time) $Q(\theta)$.

The solar sail dedicated set is a collection of solar sail orbits (all computed with the same guidance law $\overline{\mathbf{R}}(\alpha, \delta)$ till they reach the surface $Q(\theta)$:

$$S_{\overline{\mathbf{R}}(\alpha,\delta)}(\tau, \theta) = \bigcup_{\mathbf{y}_i \in \mathcal{Y}} \gamma_{\overline{\mathbf{R}}(\alpha,\delta)}(\mathbf{y}_i, \tau, \theta). \tag{13}$$

According to the definition in Eq. (13), the solar sail dedicated set is made up by orbits that

reach $Q(\theta)$ at different times, although all orbits have the same solar sail constant attitude. The cut, in the phase space, of the solar sail dedicate set with the surface $Q(\theta)$ is named $\partial S_{\overline{\mathbf{R}}(\alpha,\delta)}(\tau,\epsilon,\theta)$.

The solar sail dedicated set in Eq. (13) is associated to a generic domain of admissible initial conditions $\mathcal{Y}$; it will be shown in the following how $\mathcal{Y}$ can be defined for solar sail departure and arrival sets, from and to selected periodic orbits, respectively. Thanks to the definition of $S_{\overline{\mathbf{R}}(\alpha,\delta)}(\tau,\theta)$, the solar sail acceleration can be incorporated in a three-body frame using the same methodology developed for the invariant manifolds. More specifically, invariant manifolds and solar sail trajectories are replaced by dedicated sets which are manipulated to find connection points on suitable surfaces of section. The idea is to reproduce the role acted by invariant manifolds.

C. Solar Sail Departure Sets

In this paper, the initial orbits are LPOs in the Sun–Earth CRTBP, belonging to the northern Halo and to the planar Lyapunov families. The orbital amplitude ($\hat{A}$) or the energy level of the final periodic orbits ($\mathcal{C}$) are assumed as given by mission requirements (see Tab. 1).

In detail, the initial state of the transfers, $\mathbf{y}_i$, can be any point that belongs to the selected LPOs, slightly perturbed along the direction of the unstable eigenvector of the periodic orbit monodromy matrix. Therefore, the initial point is the generic departing point

$$\mathbf{y}_i = \mathbf{y}_i(\tau_O^D) = \phi(\mathbf{y}_O^D, 0; \tau_O^D) - \varepsilon \mathbf{v}_u, \tag{14}$$

and is found by flowing the initial nominal point $\mathbf{y}_O^D$ for a time $\tau_O^D \leq P_O^D$, being P_O the initial orbit period and adding the small perturbation $\varepsilon = 1.0 \times 10^{-6}$ along the unstable eigenvector $\mathbf{v}_s$ to generate the interior branch of the L_1-region manifold. The subscript $(\cdot)_O$ stands for the specific departure LPO selected.

The domain of admissible initial states is then written as follows

$$\mathcal{Y}^D = \{\mathbf{y}_i(\tau_O^D) | \tau_O^D \in [0, P_O^D]\}, \tag{15}$$

and the periodic orbit solar sail departure set, for some $\alpha_D \neq 90$ deg, $\tau_D > 0$, is given by the forward integration

$$D^{\mathrm{O}}_{\overline{\mathbf{R}}(\alpha_D,\delta_D)}(\tau_D,\theta_D) = \bigcup_{\mathbf{y}_i \in \mathcal{Y}^D} \gamma_{\overline{\mathbf{R}}(\alpha_D,\delta_D)}(\mathbf{y}_i,\tau_D,\theta_D). \tag{16}$$

When the cone angle $\alpha_D = 90$ deg, there is no solar sail acceleration ($\tau_D = 0$) and the classic unstable manifolds of the relative LPOs are found as $W^{\mathrm{O}}_{\overline{\mathbf{0}}(90,\delta_D)}(0,\theta_D)$, directly

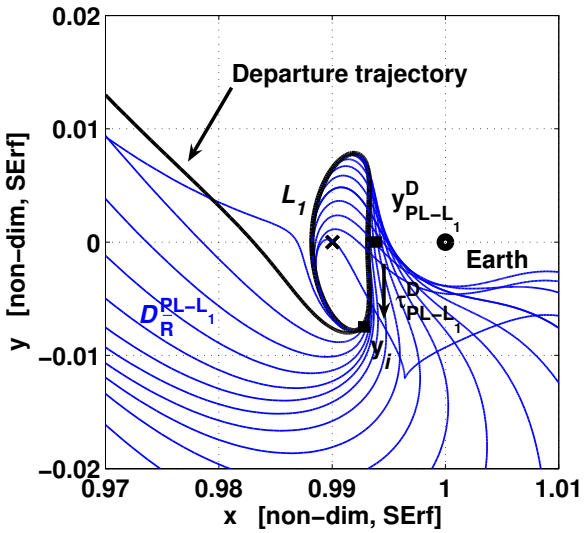

(a) Earth-to-Venus scenario: departure libration point orbit.

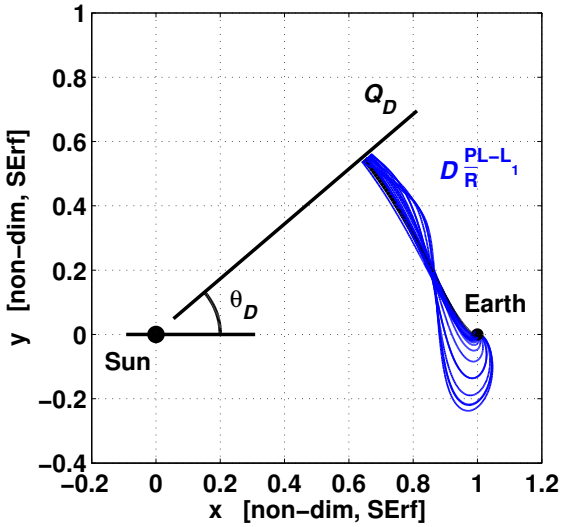

(b) Earth-to-Venus scenario: departure solar sail set.

Figure 6. Earth-to-Venus scenario: departure conditions and design variables. The blue solid lines represent the departure solar sail set $D^{\mathbf{PL\text{-}L_1}}_{\overline{\mathbf{R}}(\alpha_D,\delta_D)}(\tau_D,\theta_D)$.

following from Eq. (16). The cut, in the phase space, of the periodic orbit solar sail departure set with the surface $Q_D(\theta_D)$ is named $\partial D^{\mathrm{O}}_{\overline{\mathbf{R}}(\alpha_D,\delta_D)}(\tau_D,\theta_D)$, while the cut of the set describing the classic unstable manifold trajectories is named $\partial W^{\mathrm{O}}_{\overline{\mathbf{0}}(90,\delta_D)}(0,\theta_D)$.

D. Solar Sail Arrival Sets

As far as it concerns the target orbits, they are periodic orbits in the Sun–Venus CRTBP, belonging to the planar Lyapunov and DPO families. The orbital amplitude ($\hat{A}$) or the energy level of the final periodic orbits ($\mathcal{C}$) are assumed as given by mission requirements (see Tab. 1).

In detail, the final state of the transfers, $\mathbf{y}_f$, can be any point that belongs to the selected LPOs or DPOs, slightly perturbed along the direction of the stable eigenvector of the periodic orbit monodromy matrix. Therefore, the final point is the generic insertion point

$$\mathbf{y}_f = \mathbf{y}_f(\tau_O^A) = \phi(\mathbf{y}_O^A, 0; \tau_O^A) \pm \varepsilon \mathbf{v}_s, \tag{17}$$

and is found by flowing the initial nominal point $\mathbf{y}_O^A$ for a time $\tau_O^A \leq P_O^A$, being P_O^A the final orbit period and adding the small perturbation $\varepsilon = 1.0 \times 10^{-6}$ along the stable eigenvector $\mathbf{v}_s$ to generate the exterior branch of the L_2-region manifold. The subscript $(\cdot)_O$ stands for the specific arrival LPO or DPO selected.

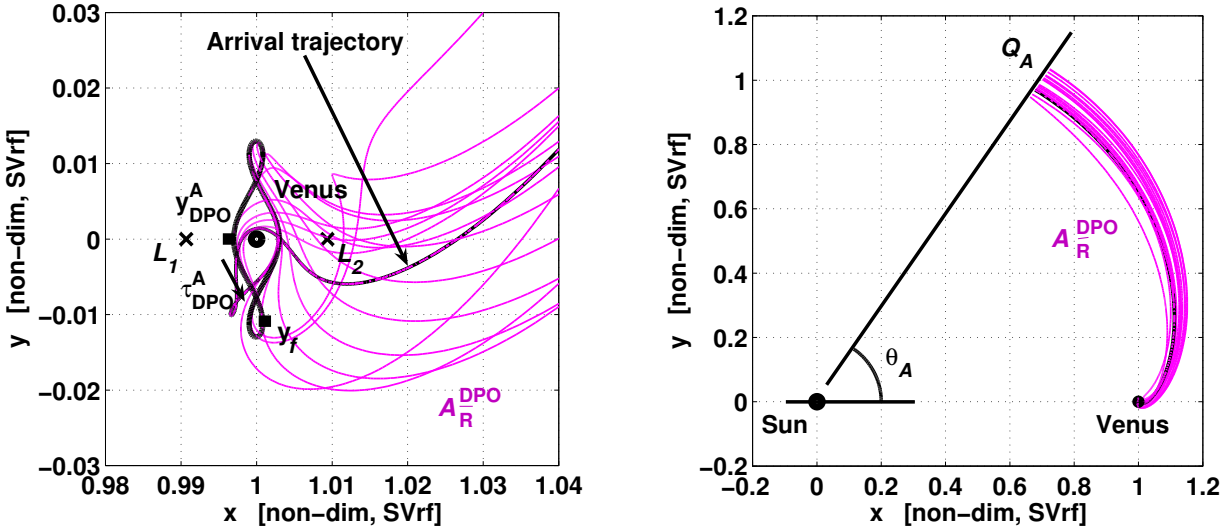

(a) Earth-to-Venus scenario: arrival libration point orbit.

(b) Earth-to-Venus scenario: arrival solar sail set.

Figure 7. Earth-to-Venus scenario: arrival conditions and design variables. The magenta solid lines represent the arrival solar sail set $A^{\mathbf{DPO}}_{\overline{\mathbf{R}}(\alpha_A,\delta_A)}(-\tau_A,\theta_A)$.

The domain of admissible final states is then written as follows

$$\mathcal{Y}^A = \{\mathbf{y}^A_f(\tau_O)|\tau^A_O \in [0, P^A_O]\}, \tag{18}$$

and the periodic orbit solar sail arrival set, for some $\alpha_A \neq 90$ deg, $\tau_A > 0$, is given by the backward integration

$$A^{\mathrm{O}}_{\overline{\mathbf{R}}(\alpha_A,\delta_A)}(-\tau_A,\theta_A) = \bigcup_{\mathbf{y}_f\in\mathcal{Y}^A} \gamma_{\overline{\mathbf{R}}(\alpha_A,\delta_A)}(\mathbf{y}_f,-\tau_A,\theta_A). \tag{19}$$

When the cone angle $\alpha_A = 90$ deg, there is no solar sail acceleration ($\tau_A = 0$) and the classic stable manifolds of the relative LPOs are found as $W^{\mathrm{O}}_{\overline{\mathbf{0}}(90,\delta_A)}(-0,\epsilon_A,\theta_A)$, directly following from Eq. (19). The cut, in the phase space, of the periodic orbit solar sail arrival set with the surface $Q_A(\theta_A)$ is named $\partial A^{\mathrm{O}}_{\overline{\mathbf{R}}(\alpha_A,\delta_A)}(-\tau_A,\theta_A)$, while the cut of the set describing the classic stable manifold trajectories is named $\partial W^{\mathrm{O}}_{\overline{\mathbf{0}}(90,\delta_A)}(-0,\theta_A)$.

IV. Transfer Design Technique

In this section, the transfer mechanism to design solar sail heteroclinic connections is described. The key idea to generate first guess solutions is to replace invariant manifolds with solar sail dedicated sets, and to manipulate the latter in the same way the manifolds are used to design space transfers.[8] With the inclusion of the solar sail acceleration and keeping

the attitude of the solar sail constant - throughout the complete transfer - with respect to the Sun-sail line, intersections between restricted three-body models can be found on suitable Poincaré sections, also for the Earth-to-Venus case. Therefore, the propellant-free feature of solar sails is combined with the exploitation of the n-body problems' intrinsic dynamics with a view of generating efficient trajectories. In detail, the technique to build first guesses, with the introduction of a few design variables, is split into basic phases as follows.

(i) The initial state of the transfers can be any point that belongs to the selected departure LPOs in the Sun–Earth CRTBP around L_1, slightly perturbed along the direction of the unstable eigenvector of the periodic orbit monodromy matrix, as stated by Eq. (14).

(ii) The initial state is then propagated forward until it intersects a suitable Poincaré surface of section $Q_D(\theta_D)$, perpendicular to the (x, y)-plane and forming an angle θ_D with the x-axis. If the trajectory is purely ballistic, then it moves along the unstable manifold of the selected LPO, i.e. on $W^{\mathrm{O}}_{\bar{\mathbf{0}}(90,\delta_D)}(0, \theta_D)$, otherwise, if solar radiation pressure is actively exploited, then it moves along the solar sail periodic orbit departure set $D^{\mathrm{O}}_{\bar{\mathbf{R}}(\alpha_D,\delta_D)}(\tau_D, \theta_D)$.

(iii) The final state of the transfers can be any point that belongs to the selected arrival LPOs around L_2 or DPOs in the Sun–Venus CRTBP , slightly perturbed along the direction of the stable eigenvector of the periodic orbit monodromy matrix, as stated by Eq. (17).

(iv) The final state is then propagated backward until it intersects a suitable Poincaré surface of section $Q_A(\theta_A)$, perpendicular to the (x, y)-plane and forming an angle θ_A with the x-axis. If the trajectory is purely ballistic, then it moves along the stable manifold of the selected LPO or DPO, i.e. on $W^{\mathrm{O}}_{\bar{\mathbf{0}}(90,\delta_A)}(-0, \theta_A)$, otherwise, if solar radiation pressure is actively exploited, then it moves along the solar sail periodic orbit arrival set $A^{\mathrm{O}}_{\bar{\mathbf{R}}(\alpha_A,\delta_A)}(-\tau_A, \theta_A)$.

(v) It is worth underlining that, as the dynamical systems under consideration are different for the two legs of the transfers, a proper operator $\mathcal{T}$ is introduced in order to map states of the arrival dynamical model (Sun–Venus) into the departure one (Sun–Earth). At this phase of the design process, thanks to the mutual independence of the dynamical models, the departure Poincaré section $Q_D(\theta_D)$ and the arrival one $Q_A(\theta_A)$ (after the proper transformation) can be arbitrarily superimposed. After this, on the same SE suitable Poincaré section $Q(\theta)$, the transit point between the solar sail departure set (phase (ii)) and the arrival one (phase (iv)) is searched for, by wisely tuning the introduced design variables.

Table 2. Values of the design variables for the generation of interplanetary (Earth PL to Venus DPO, Earth NH to Venus VL) heteroclinic first guess connections.

Applicative Scenario	τ_O^D [−, SErf]	α [deg]	δ [deg]	θ_D [deg]	τ_O^A [−, SMrf]	θ_A [deg]
Earth PL to Venus DP0	2.3577	+59.0	-90.0	+40.0	0.3346	+55.0
Earth NH to Venus VL	2.4310	+59.0	-90.0	+40.0	1.1741	+55.0

As for the mapping, for both applicative scenarios, the operator $\mathcal{T}$ is introduced: 1) the states of the arrival Sun–Venus model are written in the inertial reference frame with origin at the Sun; 2) the scaled variables are firstly transformed into physical coordinates; 3) the variables are then scaled considering the departure physical constants; 4) the variables are reported into the classic Sun–Earth rotating frame.

As first guess solutions are being generated at this stage (to be later optimized in more accurate dynamical models), small discontinuities (less than 1.0×10^{-4}) can be tolerated when looking for the patching point.

In summary, the eleven design variables necessary to search for the transfer point and therefore to build the first guess solution are (see Tab. 2):

- τ_O^D, the time parameter describing the leaving point on the initial LPO (phase (i));
- α_D, the solar sail cone angle, departure phase (phase (ii));
- δ_D, the solar sail clock angle, departure phase (phase (ii));
- θ_D, the Poincaré section angle (phase (ii),(v)) of the departure leg of the transfer;
- τ_O^A, the time parameter describing the insertion point on the final LPO (phase (iii));
- α_A, the solar sail cone angle, arrival phase (phase (iv));
- δ_A, the solar sail clock angle, arrival phase (phase (iv));
- θ_A, the Poincaré section angle (phase (iv), (v)) of the arrival leg of the transfer;
- β, the solar sail lightness number (used in Eq. (10)).

Actually, the set of design variables can be reduced by two when a solar sail constant attitude is considered throughout the complete transfers, i.e. $\alpha_D = \alpha_A = \alpha$, $\delta_D = \delta_A = \delta$. Finally, a constant value of $\beta = 0.050$ is assumed as given by mission requirements.

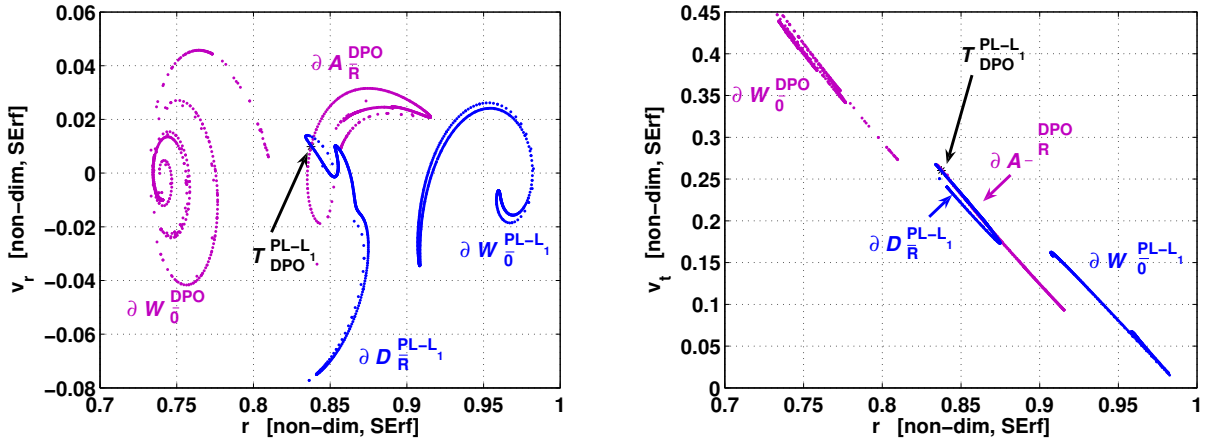

(a) Earth PL to Venus DPO scenario: Poincaré (r, v_r)-section.

(b) Earth PL to Venus DPO scenario: Poincaré (r, v_t)-section.

Figure 8. Phase space on the suitable SE Poincaré sections to design the first guess Earth PL to Venus DPO heteroclinic connection. The blue dotted line stands for the cut of the unstable manifold $\partial W^{\mathbf{PL\text{-}L_1}}_{\bar{\mathbf{0}}(90,\delta)}(0,\theta_D)$, while the other blue dotted line represents the departure solar sail set $\partial D^{\mathbf{PL\text{-}L_1}}_{\bar{\mathbf{R}}(\alpha,\delta)}(\tau_D,\theta_D)$, both for the initial planar Lyapunov orbit around L_1 of the Sun–Earth system. The magenta dotted line stands for the cut of the stable manifold $\partial W^{\mathbf{DPO}}_{\bar{\mathbf{0}}(90,\delta)}(0,\theta_A)$, while the other magenta dotted line represents the arrival solar sail set $\partial D^{\mathbf{DPO}}_{\bar{\mathbf{R}}(\alpha,\delta)}(-\tau_A,\theta_A)$, both for the final DPO around Venus of the Sun–Venus system. Finally, $T^{\mathbf{PL\text{-}L_1}}_{\mathbf{DPO}}$ is the transit point.

As described in phase (v), the departure and arrival dynamical models are disjoint, and therefore a transit point in the phase space can be found following the procedure aforementioned. But, being interested in generating initial guesses for interplanetary homoclinic connections, once the geometry of the transfer are defined patching together the two applicable restricted three-body systems, the launch epoch that enables the connection - in the real ephemeris model - is found by means of a systematic search.

A. Earth PL to Venus DPO Transit Point

The procedure described in the previous section is applied to the Earth PL to Venus DPO mission scenario, in order to design a sample feasible first guess solution, as a function of the corresponding design variables reported in Tab. 2. The departure orbit is a planar Lyapunov orbit around L_1 of the Sun–Earth model, while the arrival one is a DPO around Venus of the Sun–Venus model (see Tab. 1). Basically, the solar sail flies on the interior SE dedicated solar sail departure set till it is captured on the exterior SV dedicated solar sail arrival set.

In Fig. 8 are shown the cuts of the LPO unstable manifold trajectories of the Sun–Earth model, namely $\partial W^{\text{PL-L}_1}_{\bar{\mathbf{0}}(90,\delta)}(0,\theta_D)$, and of the solar sail departure dedicated set $\partial D^{\text{PL-L}_1}_{\bar{\mathbf{R}}(\alpha,\delta)}(\tau_D,\theta_D)$, both for the initial planar Lyapunov orbit around L_1, on the suitable Poincaré sections.

Moreover, on the same suitable Poincaré sections, Fig. 8 presents the cuts of the stable

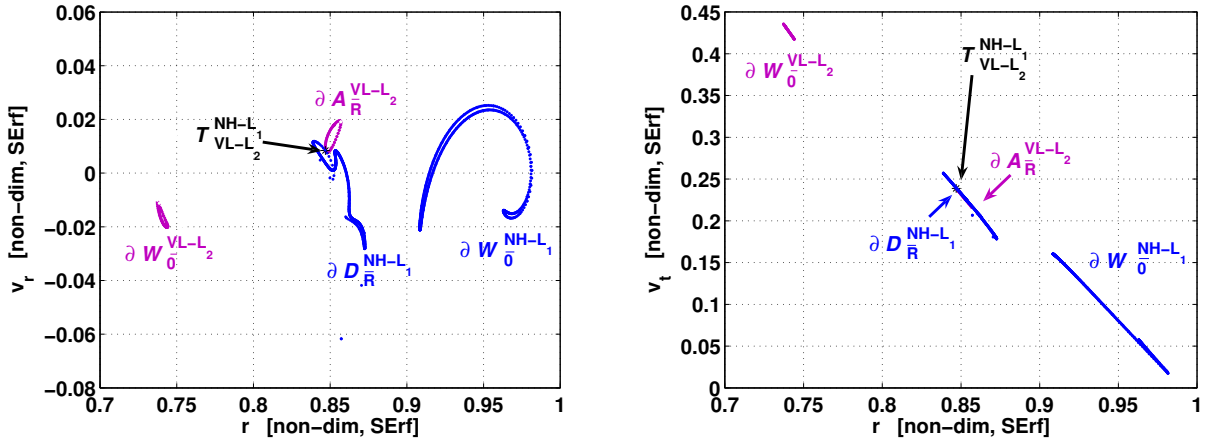

(a) Earth NH to Venus VL scenario: Poincaré (r, v_r)-section.

(b) Earth NH to Venus VL scenario: Poincaré (r, v_t)-section.

Figure 9. Phase space on the suitable SE Poincaré sections to design the first guess Earth NH to Venus VL heteroclinic connection. The blue dotted line stands for the cut of the unstable manifold $\partial W^{\mathbf{NH\text{-}L_1}}_{\bar{\mathbf{0}}(90,\delta)}(0, \theta_D)$, while the other blue dotted line represents the departure solar sail set $\partial D^{\mathbf{NH\text{-}L_1}}_{\bar{\mathbf{R}}(\alpha,\delta)}(\tau_D, \theta_D)$, both for the initial northern Halo orbit around L_1 of the Sun–Earth system. The magenta dotted line stands for the cut of the stable manifold $\partial W^{\mathbf{VL\text{-}L_2}}_{\bar{\mathbf{0}}(90,\delta)}(0, \theta_A)$, while the other magenta dotted line represents the arrival solar sail set $\partial D^{\mathbf{VL\text{-}L_2}}_{\bar{\mathbf{R}}(\alpha,\delta)}(-\tau_A, \theta_A)$, both for the final southern Halo orbit around L_2 of the Sun–Venus system. Finally, $T^{\mathbf{NH\text{-}L_1}}_{\mathbf{VL\text{-}L_2}}$ is the transit point.

manifold trajectories of the Sun–Venus model $\partial W^{\mathrm{DPO}}_{\bar{\mathbf{0}}(90,\delta)}(-0, \theta_A)$ and of the solar sail arrival dedicated set $\partial A^{\mathrm{DPO}}_{\bar{\mathbf{R}}(\alpha,\delta)}(-\tau_A, \theta_A)$, both for the final DPO around Venus. The cuts are shown on the (r, v_r)-section and (r, v_t)-section.

For reasonable transfer times, the ballistic manifold structure of the SE and the SV models do not intersect; on the other hand, the Earth PL to Venus DPO heteroclinic first guess solution corresponds to the intersection point

$$T^{\text{PL-L}_1}_{\text{DPO}} \doteq \partial D^{\text{PL-L}_1}_{\bar{\mathbf{R}}(\alpha,\delta)}(\tau_D, \theta_D) \cap \partial A^{\text{DPO}}_{\bar{\mathbf{R}}(\alpha,\delta)}(-\tau_A \theta_A). \tag{20}$$

In the generation process of the first guess solution (to be later optimized in more sophisticated models), small discontinuities (in the out-of-plane components) can be tolerated when looking for the transit point.

B. Earth NH to Venus VL Transit Point

As far as it concerns the Earth NH to Venus VL scenario, the same procedure described previously is implemented, in order to design a sample feasible first guess solution, as a function of the corresponding design variables reported in Tab. 2. In this case, the departure orbit is a northern Halo orbit around L_1 of the Sun–Earth model, while the arrival one is a

Table 3. Transfer performances of the interplanetary (Earth PL to Venus DPO, Earth NH to Venus VL) heteroclinic first guess connections.

Applicative Scenario	Departure Date	Arrival Date	Tof [years]	β [–]
Earth PL to Venus DPO	2021/Jan/01	2022/Sep/04	1.6738	0.050
Earth NH to Venus VL	2020/Nov/20	2022/Aug/24	1.7851	0.050

vertical Lyapunov around L_2 of the Sun–Venus model (see Tab. 1). Basically, the solar sail flies on the interior SE dedicated solar sail departure set till it is captured on the exterior SV dedicated solar sail arrival set.

In Fig. 9 are represented the cuts of the LPO unstable manifold trajectories of the Sun–Earth model, $\partial W^{\text{NH-L}_1}_{\overline{\mathbf{0}}(90,\delta)}(0,\theta_D)$ and of the solar sail departure dedicated set $\partial D^{\text{NH-L}_1}_{\overline{\mathbf{R}}(\alpha,\delta)}(\tau_D,\theta_D)$, both for the initial northern Halo orbit around L_1, on the suitable Poincaré sections.

Furthermore, on the same suitable Poincaré sections, in Fig. 9 are shown the cuts of the stable manifold trajectories of the Sun–Venus model $\partial W^{\text{VL-L}_2}_{\overline{\mathbf{0}}(90,\delta)}(-0,\theta_A)$ and of the solar sail arrival dedicated set $\partial A^{\text{VL-L}_2}_{\overline{\mathbf{R}}(\alpha,\delta)}(-\tau_A,\theta_A)$, both for the final vertical Lyapunov orbit around L_2. The cuts are shown on the (r,v_r)-section and (r,v_t)-section.

As expected, the pure ballistic manifolds of the SE and the SV models do not intersect; on the other hand, the Earth NH to Venus VL heteroclinic first guess solution corresponds to the intersection point

$$T^{\text{NH-L}_1}_{\text{VL-L}_2} \doteq \partial D^{\text{NH-L}_1}_{\overline{\mathbf{R}}(\alpha,\delta)}(\tau_D,\theta_D) \cap \partial A^{\text{VL-L}_2}_{\overline{\mathbf{R}}(\alpha,\delta)}(-\tau_A,\theta_A). \tag{21}$$

Again, in the define process of the first guess solution (to be later optimized in more accurate models), small discontinuities (in the out-of-plane components) can be admitted when looking for the transit point.

C. Preliminary Transfer Solutions

Some preliminary transfer solutions of the Earth PL to Venus DPO and Earth NH to Venus VL transfers are presented in Fig. 10 and Fig. 11, respectively. Moreover, preliminary transfer performances are reported in Tab. 3.

While Fig. 10(a) shows the transfer in the Sun–Earth synodic reference frame and Fig. 10(a) shows the transfer in the Sun–Venus synodic reference frame, Fig. 11(a) and Fig. 11(b) use a heliocentric inertial reference frame and also provide information on the solar sail acceleration vector through the use of arrows.

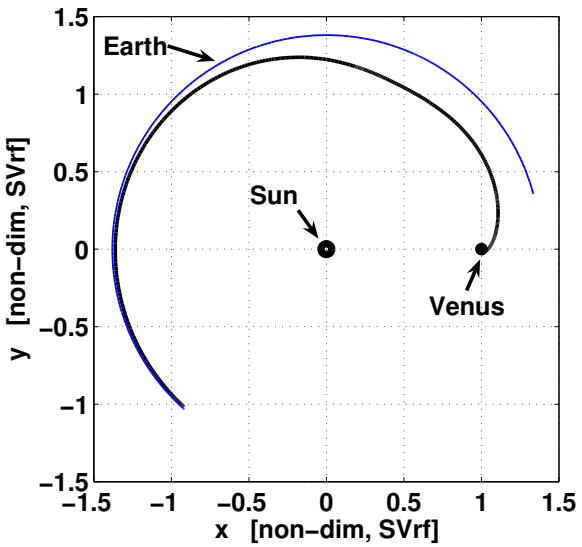

(a) Earth PL to Venus DPO scenario: transfer trajectory in the Sun–Venus rotating frame.

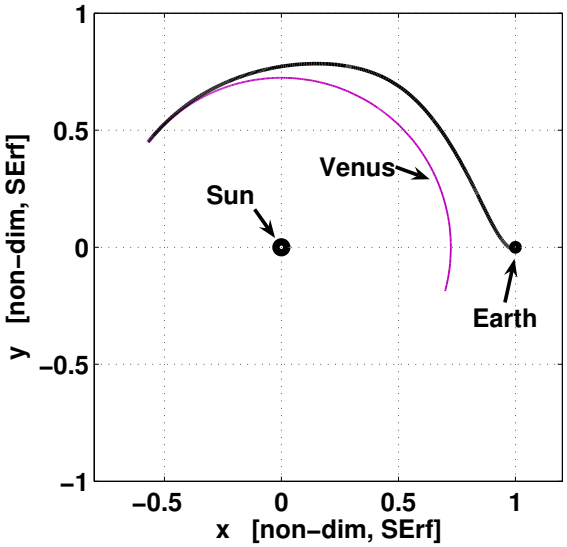

(b) Earth NH to Venus VL scenario: transfer trajectory in the Sun–Earth rotating frame.

Figure 10. Applicative scenarios investigated: preliminary transfer trajectories in the Sun–Earth and Sun–Venus rotating frames.

As for the flight time, they are less than a couple years, as expected flying along a manifold-like type of trajectories. For the Earth PL to Venus DPO case, the transfer lasts less more than 1.7 years, while for the Earth NH to Venus VL case, it lasts slightly less than 1.8 years.

V. Trajectory Optimisation

As stated in the introduction, the starting periodic orbit and the target one are defined in different CRTBP. The first and second phases of the transfer connecting these LPOs or DPOs will therefore also be defined in different CRTBPs.

A. The Controlled Bi-Circular Restricted Four-Body Problem

In order for the dynamics to be consistent throughout the transfer, a fourth body perturbation is included. Therefore, for the Earth-to-Venus transfer scenario, Venus will be the fourth body in the departure Sun–Earth CRTBP, while the Earth will be the fourth body in the arrival Sun–Venus CRTBP.

The model used to take into account solar sail acceleration and the gravitational attractions of all the celestial bodies involved in the design process is the controlled bi-circular

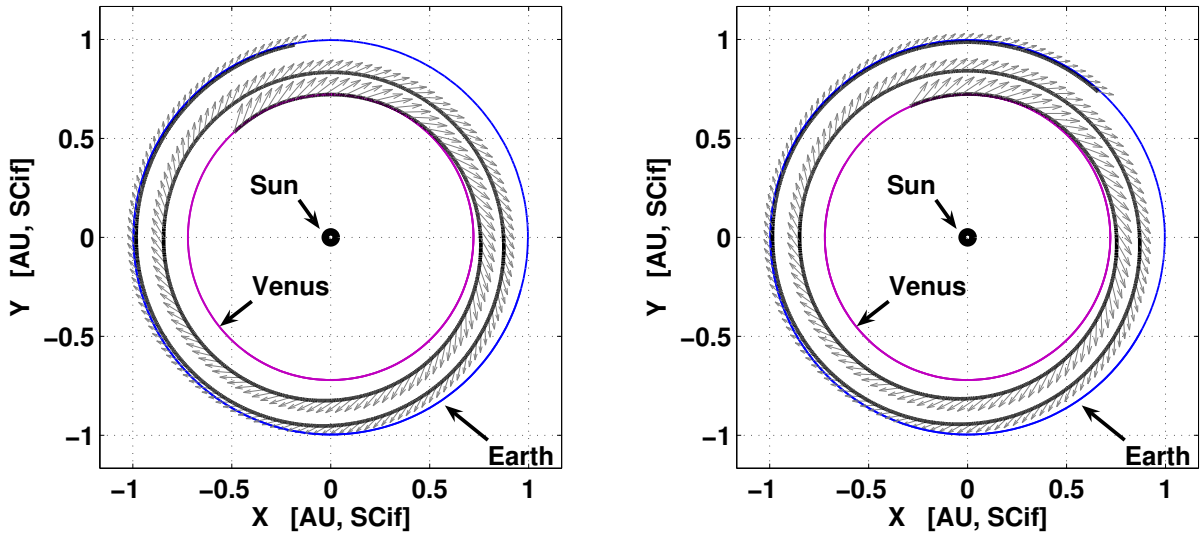

(a) Earth PL to Venus DPO scenario: transfer trajectory in the Sun–centered inertial frame.

(b) Earth NH to Venus VL scenario: transfer trajectory in the Sun–centered inertial frame.

Figure 11. Applicative scenarios investigated: preliminary transfer trajectories in the Sun-Centered inertial frame.

restricted four body problem BCRFBP:

$$\ddot{x} - 2\dot{y} = \frac{\partial \Omega_F}{\partial x} + a_s s_x, \qquad \ddot{y} + 2\dot{x} = \frac{\partial \Omega_F}{\partial y} + a_s s_z, \qquad \ddot{z} = \frac{\partial \Omega_F}{\partial z} + a_s s_z, \qquad \dot{\varphi} = \omega_F, \quad (22)$$

where $\hat{\mathbf{s}} = (s_x, s_y, s_z)^\top$ and a_s have already been defined in section A. The four-body potential Ω_F reads

$$\Omega_F(x, y, z, \varphi, \mu) = \Omega_T(x, y, z, \mu) + \frac{m_F}{r_F} - \frac{m_F}{\rho_F^2}(x \cos\varphi + y \sin\varphi). \quad (23)$$

The dimensionless physical constants introduced to describe the fourth body perturbation are in agreement with those of the reference three-body model.

In the first phase, the distance between Venus and the Sun–Earth barycenter is $\rho_F = 7.2391 \cdot 10^{-1}$, the mass of Venus is $m_F = 2.4471 \cdot 10^{-6}$, and its angular velocity with respect to the SE rotating frame is $\omega_F = 6.2356 \cdot 10^{-1}$. In the second phase, the distance between Earth and the Sun–Venus barycenter is $\rho_F = 1.3814 \cdot 10^{1}$, the mass of Earth is $m_F = 3.0035 \cdot 10^{-6}$, and its angular velocity with respect to the SV rotating frame is $\omega_F = -3.8407 \cdot 10^{-1}$.

The general location of the fourth body is located at $(\rho_F \cos\varphi, \rho_F \sin\varphi, 0)$, and therefore the distance between the fourth body and the spacecraft is calculated as

$$r_F^2 = (x - \rho_F \cos\varphi)^2 + (y - \rho_F \sin\varphi)^2 + z^2. \quad (24)$$

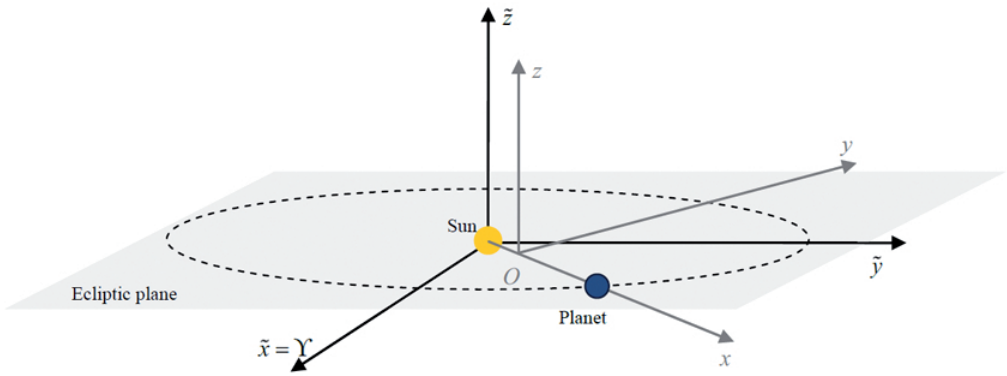

Figure 12. Schematic of circular ecliptic ephemerides of planets and definition of heliocentric inertial reference frame $(\tilde{x}, \tilde{y}, \tilde{z})$, and Sun-planet synodic reference frame (x, y, z).

B. Ephemerides

The inclusion of the fourth-body perturbation transforms the autonomous CRTBP into a non-autonomous problem through the angle ϕ. The actual relative position of the planets thus comes into play and is approximated through a simple circular, ecliptic ephemeris. This means that all planets are assumed to orbit the Sun in circular orbits (as holds in the CRTBP) and in the ecliptic plane (see Fig. 12).

To describe the ephemerides, an inertial heliocentric reference frame is employed: the $\tilde{x}$-axis points towards the vernal equinox, the $\tilde{z}$-axis is perpendicular to the ecliptic plane and the $\tilde{y}$-axis completes the right-handed reference frame. In dimensional form, the ephemerides of the planets are then given by:

$$\tilde{\mathbf{r}}_P = \begin{bmatrix} \cos\varphi_0 + \dot{\varphi}\tilde{t}_{MJD2000,s} \\ \sin\varphi_0 + \dot{\varphi}\tilde{t}_{MJD2000,s} \\ 0 \end{bmatrix}, \quad \tilde{\mathbf{r}}_P = \sqrt{\frac{\mu_S}{\lambda}} \begin{bmatrix} -\sin\varphi_0 + \dot{\varphi}\tilde{t}_{MJD2000,s} \\ \cos\varphi_0 + \dot{\varphi}\tilde{t}_{MJD2000,s} \\ 0 \end{bmatrix}, \tag{25}$$

with $\dot{\varphi} = 1/\tau$ and φ_0 the angular position of the planet at a reference epoch which is chosen to be 2000/Jan/01, similar to the MJD2000 notation. The time $\tilde{t}_{MJD2000,s}$ in Eqs. (25) is the time in seconds after 2000/Jan/01 (i.e. $\tilde{t}_{MJD2000,s} = 0$ corresponds to 2000/Jan/01). The angular position of the planet at this reference epoch is calculated using the analytical ephemerides implemented in the Matlab® function uplanet.m[a] that was successfully verified against the JPL/NAIF/SPICE de405 ephemerides. Note that the assumption of circular, ecliptic ephemerides imposes little inaccuracies for Venus (eccentricity $e = 0.0067$, and inclination $i = 3.35\,\text{deg}$). However, the purpose of the current work is to demonstrate the concept.

[a]Dysli, P. 1977. Analytical Ephemeris for Planets (Matlab® code *uplanet.m*).

Future work will therefore consider more realistic and accurate planetary ephemerides.

C. Reference Frame Transformations

Since the ephemeris in Eqs. (25) only provides the position and velocity of the fourth-body in an heliocentric inertial reference frame, a transformation is required to obtain the planet's state vector in the Sun-planet synodic reference frame for use in Eqs. (22).

The general transformation of a state vector $\tilde{\mathbf{x}} = [\tilde{\mathbf{r}}\ \dot{\tilde{\mathbf{r}}}]^\top$ in the heliocentric inertial reference frame to a state vector $\mathbf{x} = [\mathbf{r}\ \dot{\mathbf{r}}]^\top$ in the Sun-planet synodic reference frame is given through the following set of equations:

$$\varphi = \tan 2^{-1}\left(\frac{\tilde{\mathbf{r}}_{P,y}}{\tilde{\mathbf{r}}_{P,x}}\right), \tag{26}$$

$$\mathbf{R}_z = \begin{bmatrix} \cos\varphi & \sin\varphi & 0 \\ -\sin\varphi & \cos\varphi & 0 \\ 0 & 0 & 1 \end{bmatrix}, \tag{27}$$

$$\mathbf{r}' = \mathbf{R}_z\tilde{\mathbf{r}}, \tag{28}$$

$$\dot{\mathbf{r}} = \mathbf{R}_z\dot{\tilde{\mathbf{r}}} + \overline{\omega}\times\mathbf{r}', \tag{29}$$

$$\mathbf{r} = \mathbf{r}' + [\mu\ 0\ 0]^\top, \tag{30}$$

where the matrix $\mathbf{R}_z$ rotates the $\tilde{x}$-axis of the heliocentric inertial reference frame onto the x-axis of the Sun-planet synodic reference frame and Eqs. (29), Eqs. (30) account for the rotational velocity of the synodic reference frame and translates the origin from the Sun to the barycentre. A simple relationship also exists between the dimensional $\tilde{t}_{MJD2000,s}$ in the heliocentric inertial reference frame and the dimensionless time t in the Sun-planet synodic reference frame. By defining $t = \tilde{t}_{MJD2000,s} = 0$ to be 2000/Jan/01, $t = 2\pi$ corresponds to $\tilde{t}_{MJD2000,s} = 2\pi/\tau$, or equivalently: 2001/Jan/01 in the Sun–Earth problem, 2000/Aug/21 in the Sun–Venus problem.

D. Direct Pseudospectral Method

The first guess connections discussed previously reveal to be sub-optimal as there could be minor discontinuities in position and velocities at the transit points between the two three-body systems. In summary, the discontinuities can be solved by transferring the first-guess trajectories to a direct pseudospectral method, which discretises the time interval into a finite number of collocation points and uses Legendre or Chebyshev polynomials to approximate

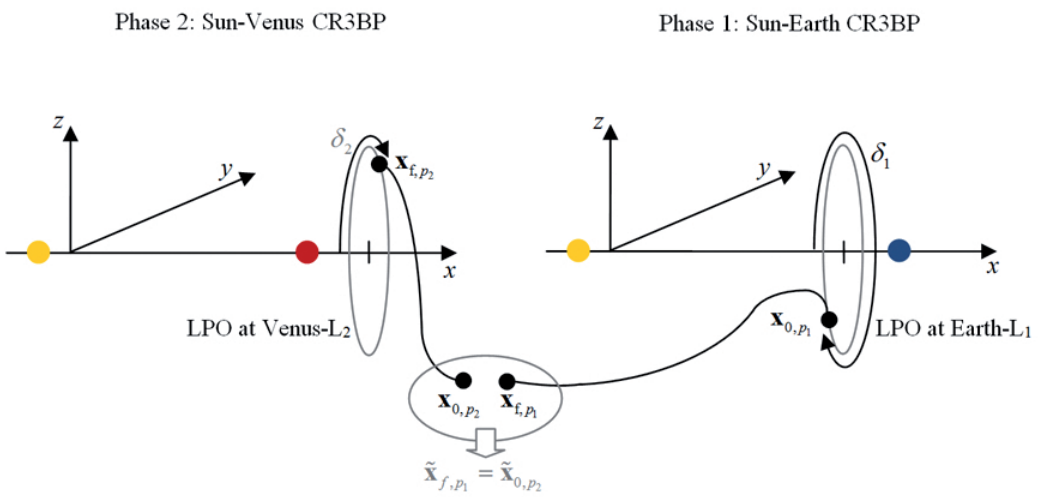

Figure 13. Illustration of two-phase approach for the Earth-to-Venus transfer and definition of static optimisation parameters δ_1 and δ_2.

and interpolate the time dependent variables at the collocation points. This way, the infinite dimensional optimal control problem is transformed into a finite dimension non-linear programming (NLP) problem. Pseudospectral methods have become increasingly of interest for solving optimal control problem because the characteristics of the orthogonal polynomials are very well suited to the mathematical operations required to solve the optimal control problem: functions can be very accurately approximated, derivatives of the state functions at the nodes are computed by matrix multiplication only and any integral associated with the problem is approximated using well-known Gauss quadrature rules. This, together with the fact that pseudospectral methods have a rapid rate of convergence (i.e. convergence to a very accurate solution with few number of nodes), is the reason for using pseudospectral methods, where a particular implementation of a direct pseudospectral method is chosen, i.e. PSOPT.[24] PSOPT is an open source tool developed by Victor M. Becerra of the University of Reading and is written in C++ and is interfaced to IPOPT (Interior Point OPTimizer)[25] to solve the NLP problem. Moreover, PSOPT can deal with all optimal control problem elements defined above: multi-phase problems, phase linkage constraints, boundary constraints, path constraints, static optimisation parameters and bounds on state variables, control variables and time.

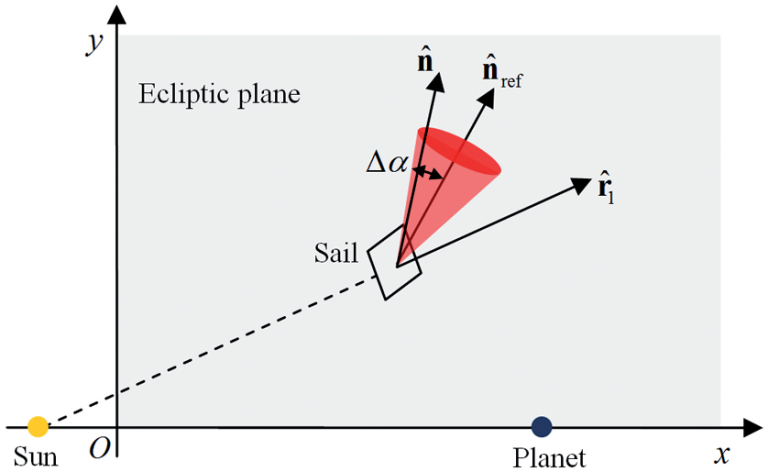

Figure 14. Illustration of solar sail limited control authority.

VI. Optimal Control Problem

According to the formalism proposed by Betts,[26] the controlled dynamics (Eqs. (22)) is written in the first-order form

$$\begin{aligned} \dot{x} &= v_x \\ \dot{y} &= v_y \\ \dot{z} &= v_z \\ \dot{v}_x &= 2v_y + \Omega_{Fx} + a_s s_x \\ \dot{v}_y &= -2v_x + \Omega_{Fy} + a_s s_y \\ \dot{v}_z &= \Omega_{Fz} + a_s s_z, \end{aligned} \tag{31}$$

with $v_x = \dot{x}$, $v_y = \dot{y}$, $v_z = \dot{z}$. In a compact explicit form, system Eqs. (31) reads

$$\dot{\mathbf{x}} = \mathbf{f}[\mathbf{x}(t), \mathbf{u}(t), \mathbf{p}, t], \tag{32}$$

where $\mathbf{f}$ is the vector field, $\mathbf{u} = a_s\hat{\mathbf{s}}$ is the solar sail acceleration, the state vector is $\mathbf{x} = \{x, y, z, v_x, v_y, v_z, \varphi\}^\top$, and $\mathbf{p}$ is a vector of parameters. The aim is finding the guidance law $\mathbf{u} = \mathbf{u}(t)$, $t \in [t_0, t_f]$, that minimizes a prescribed scalar performance index

$$J = J(\mathbf{x}, \mathbf{u}, \mathbf{p}, t), \tag{33}$$

Table 4. Earth L_1 planar Lyapunov orbit to Venus DPO transfer results.

Description	α_{ref} [deg]	δ_{ref} [deg]	Departure Date	Arrival Date	ToF [days]
Initial guess	n/a	n/a	2021/Jan/01	2022/Sep/04	610
$\Delta\alpha$ inactive	n/a	n/a	2021/Apr/30	2022/Jun/15	412
$\Delta\alpha = 20\,\text{deg}$	38.5	-96.0	2021/May/02	2022/Jun/21	415
$\Delta\alpha = 15\,\text{deg}$	39.2	-89.9	2021/Apr/24	2022/Jun/19	421
$\Delta\alpha = 10\,\text{deg}$	50.3	-91.5	2021/Apr/09	2022/Jul/16	463
$\Delta\alpha = 7.5\,\text{deg}$	53.7	-96.0	2021/Mar/28	2022/Jul/30	489
$\Delta\alpha = 5.0\,\text{deg}$	56.0	-88.5	2021/Mar/17	2022/Aug/13	515
$\Delta\alpha = 2.5\,\text{deg}$	58.0	-88.0	2021/Mar/02	2022/Aug/29	545

while satisfying certain mission constraints.[27] In this work, the aim is to minimize the time of flight,

$$J = t_f - t_0. \tag{34}$$

The control history consists of the Cartesian components of the normal vector to the solar sail (or equivalently the unit solar sail acceleration vector)

$$[-1\ -1\ -1]^\top \leq [u_x\ u_y\ u_z]^\top \leq [1\ 1\ 1]^\top. \tag{35}$$

Finally, the independent variable is the dimensionless time, t. Bounds on the initial and final time are imposed such that a 2020–2025 launch window and a 2020–2027 arrival window are ensured. In dimensionless time, these windows translate into

$$\begin{aligned} 40.0\pi &\leq t_0 \leq 50.0\pi \quad \text{Sun–Earth system} \\ 64.9\pi &\leq t_f \leq 87.7\pi \quad \text{Sun–Venus system} \end{aligned} \tag{36}$$

A. Two-Phase Approach

As indicated before, due to the fact that the initial and target LPOs and DPOs are defined in different CRTBPs, the initial and final parts of the transfer will also have to be defined in different CRTBPs. The transfer is therefore split into two phases, where the first phase (hereafter referred to through the subscript p_1) is defined in the Sun–Earth CRTBP with

Venus as fourth-body, while the second phase (referred to through the subscript p_2) is defined in the Sun–Venus CRTBP with Earth as fourth-body (see Fig. 13).

Clearly, a smooth linkage between the two phases has to exist, i.e. a smooth linkage between the final conditions of the first phase and the initial conditions of the second phase. Therefore, constraints are enforced that guarantee continuity across the linkage in terms of position, velocity, time and sail attitude. Since two different CRTBPs are linked, the relative orientation of the synodic reference frames at the time of the linkage needs to be considered. Therefore, the reverse of the transformation described in Eq. (26)–Eq. (29) is used to transform the final state vector of the first phase, $\mathbf{x}_{f,p_1}$, and the initial state vector of the second phase, $\mathbf{x}_{0,p_2}$, to the heliocentric inertial reference frame. In this reference frame, the two state vectors can be equated to ensure a continuous link between the two phases

$$\tilde{\mathbf{x}}_{f,p_1} = \tilde{\mathbf{x}}_{0,p_2}. \tag{37}$$

A similar transformation is performed to obtain a continuous link on the sail attitude such that the following constraint can be enforced

$$\tilde{\mathbf{u}}_{f,p_1} = \tilde{\mathbf{u}}_{0,p_2}. \tag{38}$$

Finally, the dimensionless time is converted to dimensional time $\tilde{t}_{MJD2000}$ to also guarantee a continuous link in terms of time

$$\tilde{t}_{MJD2000,\, f,p_1} = \tilde{t}_{MJD2000,\, 0,p_2}. \tag{39}$$

From Eq. (37)–Eq. (39) it is clear that, in total, 10 linkage constraints are enforced.

B. Boundary Constraints

To ensure that the trajectory departs from the Earth L_1 LPOs and winds onto the Venus L_2 LPO or DPO, a set of boundary constraints is imposed: the state vector at the start of phase 1, $\mathbf{x}_{0,p_1}$, should coincide with the Earth L_1 LPOs and the state vector at the end of phase 2, $\mathbf{x}_{f,p_2}$, should coincide with the Venus L_2 LPOs or DPOs. Two static optimisation parameters are used to find the optimum departure and arrival location on these LPOs. These static parameters are measured along the LPOs and are defined as $0 \leq \delta_1 \leq P_O, p_1$ and $0 \leq \delta_2 \leq P_O, p_2$ (see Fig. 13). The boundary constraints thus become

$$\mathbf{x}_{0,p_1} = \mathbf{x}_{O,p_1}(\delta_1), \tag{40}$$

$$\mathbf{x}_{f,p_2} = \mathbf{x}_{O,p_2}(\delta_2). \tag{41}$$

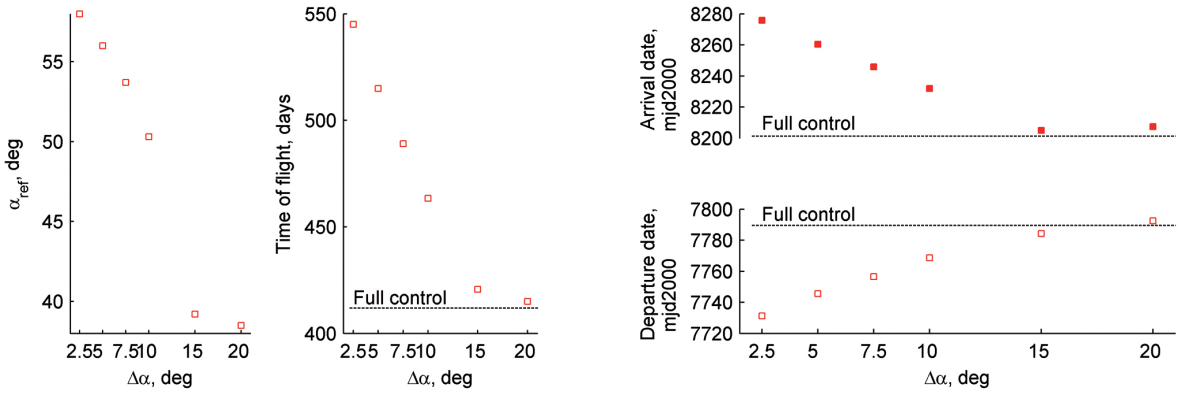

(a) Optimal sail reference attitude and time of flight.

(b) Departure and arrival times.

Figure 15. Earth L_1 planar Lyapunov orbit to Venus DPO transfers: influence of solar sail controllability, $\Delta\alpha$.

The actual values for $\mathbf{x}_{O,p_1}(\delta_1)$ and $\mathbf{x}_{O,p_2}(\delta_2)$ are computed through an interpolation of large state matrices that provide the position and velocity vectors along the LPOs for a fine mesh in δ_1 or δ_2, i.e. for a discrete number of locations along each of the LPOs or DPOs. Note that no boundary constraints are imposed on the final conditions of the first phase and the initial conditions of the second phase. The choice for the location and time of the linkage as defined in Eq. (37) and Eq. (39) are thus completely free and optimisable.

C. Path Constraints

A set of path constraints are enforced on the control vector that will hold throughout the entire trajectory, i.e. in both phases 1 and 2. First, a path constraint is introduced to ensure that the norm of the control vector is unity

$$\|\mathbf{u}\| = 1. \tag{42}$$

A second path constraint makes sure that the control vector always points away from the Sun. This has to be taken into account because a solar sail cannot generate an acceleration component in the direction of the Sun[3]

$$\hat{\mathbf{r}}_1 \cdot \hat{\mathbf{u}} \geq 0. \tag{43}$$

A final path constraint is defined to introduce limitations on the control authority of the solar sail as discussed in the introduction of this paper.

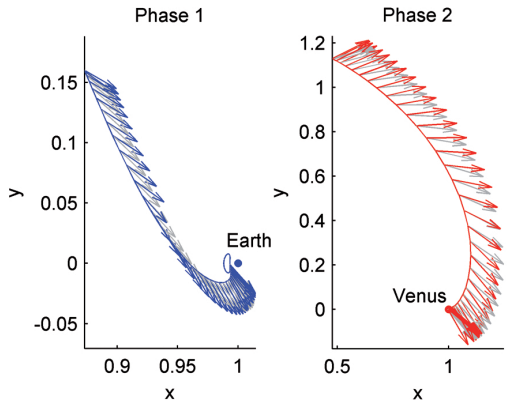

(a) Transfer phases with sail acceleration direction (color) and $\hat{\mathbf{u}}_{\text{ref}}$-direction (grey).

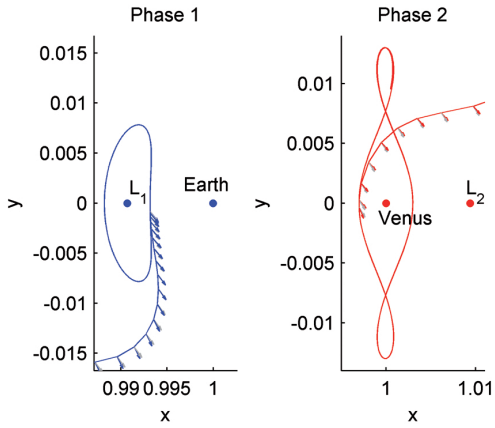

(b) Departure and arrival transfer sections.

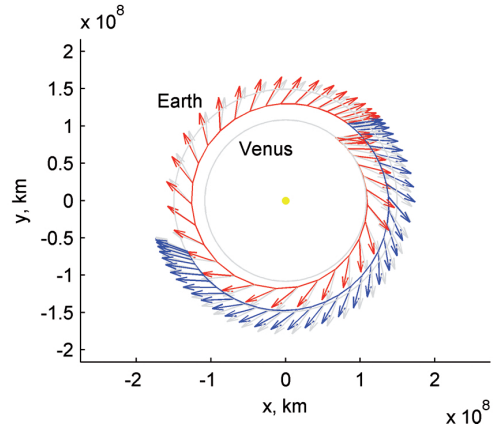

(c) Transfer in Sun-centered inertial reference frame.

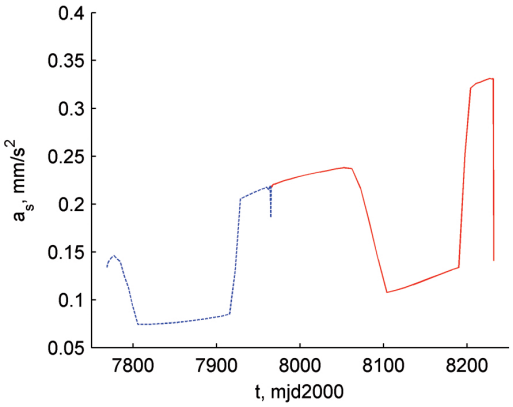

(d) Solar sail acceleration magnitude.

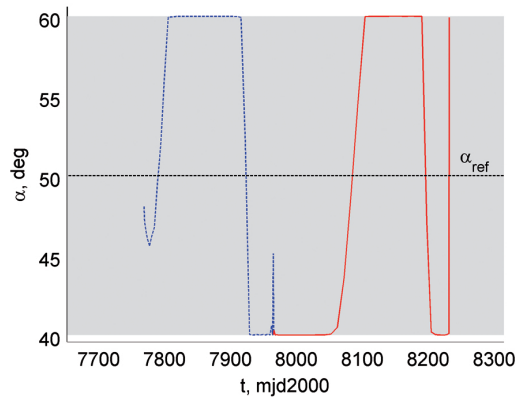

(e) Cone angle.

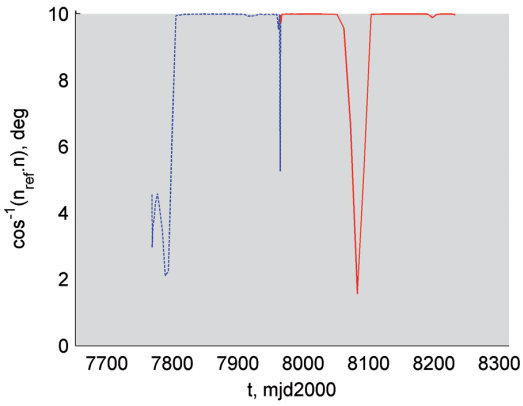

(f) Angle between $\hat{\mathbf{u}}$ and $\hat{\mathbf{u}}_{\text{ref}}$.

Figure 16. Earth L_1 planar Lyapunov orbit to Venus DPO transfer: details for $\Delta\alpha = 10\,\text{deg}$.

Table 5. Earth L_1 northern Halo to Venus L_2 vertical Lyapunov orbit transfer results.

Description	α_{ref} [deg]	δ_{ref} [deg]	Departure Date	Arrival Date	ToF [days]
Initial guess	n/a	n/a	2020/Nov/20	2022/Aug/24	650
$\Delta\alpha$ inactive	n/a	n/a	2021/Apr/30	2022/Jun/19	414
$\Delta\alpha = 20\,\text{deg}$	38.3	-67.1	2021/Apr/24	2022/Jun/14	416
$\Delta\alpha = 15\,\text{deg}$	38.7	-70.0	2021/Apr/15	2022/Jun/09	420
$\Delta\alpha = 10\,\text{deg}$	45.8	-63.2	2021/Apr/03	2022/Jul/04	458
$\Delta\alpha = 7.5\,\text{deg}$	49.1	-62.0	2021/Mar/24	2022/Jul/19	482
$\Delta\alpha = 5.0\,\text{deg}$	51.1	-59.7	2021/Mar/12	2022/Jul/31	506
$\Delta\alpha = 2.5\,\text{deg}$	50.4	-50.9	2021/Feb/15	2022/Aug/12	543

This is done by defining two more static optimisation parameters, $0 \leq \delta_3 \leq \frac{1}{2}$ and $0 \leq \delta_4 \leq 2\pi$. These static parameters describe a constant cone angle, α_{ref}, and clock angle, δ_{ref}, that define an optimal solar sail reference attitude, $\hat{\mathbf{u}}_{\text{ref}}$. To limit the control authority of the solar sail, the solar sail acceleration unit vector $\hat{\mathbf{u}}$ is now allowed to move within a cone around $\hat{\mathbf{u}}_{\text{ref}}$ with a half-angle $\Delta\alpha$ (see Fig. 14). The value for $\Delta\alpha$ is an input parameter to the optimal control problem. The associated path constraint then becomes

$$\cos^{-1}(\hat{\mathbf{u}}_{\text{ref}} \cdot \hat{\mathbf{u}}) \leq \Delta\alpha. \tag{44}$$

VII. Solar Sail Heteroclinic Transfer Connections

Using the initial guess as obtained from the solar sail dedicated sets, a range of results for the Earth L_1 planar Lyapunov orbit to Venus DPO transfer scenario and for the Earth L_1 northern Halo to Venus L_2 vertical Lyapunov orbit one are presented in this section.

A. Earth PL to Venus DPO Case

First, the results for a fully controllable sail are provided, where the constraint in Eq. (44) is omitted. This will provide the absolute minimum time of flight achievable. Subsequently, the constraint in Eq. (44) is introduced and a continuation is started where the results for a larger value for $\Delta\alpha$ are used as an initial guess to obtain the results for a smaller value for $\Delta\alpha$.

All results consist of 40 collocation points in both phases, i.e. 80 collocation points in total. The main results are summarised in Tab. 4 for both the initial guess, the fully controllable solar sail (i.e. $\Delta\alpha$ is inactive) as well as for a range of values for $\Delta\alpha$. Fig. 15 presents these results in graphical form to highlight the trend in the results: the smaller the value for $\Delta\alpha$, the more limited the controllability of the sail is. The table clearly demonstrates the effect of this limited controllability as the time of flight increases from 412 days for a fully controllable sail to 545 days for a very limited steering capability of $\Delta\alpha = 2.5\,\text{deg}$. Despite this increase of 32 percent, it is remarkable that the transfer can be executed and all constraints can be satisfied with such limited control capabilities. Note that the significant reduction in the time of flight between the initial guess and the fully controllable sail can be attributed to the fact that the initial guess considered coasting arcs at the start and end of the transfer while the time-optimal results presented here assume the use of the solar sail from the start to the end, i.e. from the Earth L_1 planar Lyapunov orbit to the Venus DPO.

Another effect of the decreasing value for $\Delta\alpha$ is an increase in the optimal cone and clock angles of the reference sail attitude, α_{ref} and δ_{ref}. The solar sail acceleration direction thus becomes more planar and tangential as the control capabilities decrease. The planar nature of the optimal solar sail reference attitude can be expected as the Lyapunov and DPO orbits are planar as well. Details of the transfer with $\Delta\alpha = 10\,\text{deg}$ are provided in Fig. 16. Plots Fig. 16(a) and Fig. 16(b) are in the synodic Sun–Earth reference frame, while plot Fig. 16(c) presents the transfer in the inertial reference frame. The detail in Fig. 16(b) shows where the transfer leaves the Earth L_1 planar Lyapunov orbit and where it winds onto the Venus DPO.

The corresponding values for the optimisation parameters δ_1 and δ_2 are: $\delta_1 = 1.6414$ and $\delta_2 = 2.1020$. The grey arrows in plots a-c indicate the optimal reference solar sail attitude, while plots e-f show the variation of the solar sail acceleration within a 10 deg half angle cone around this optimal reference attitude. It is clear from plot f that the upper bound on the constraint in Eq. (44) is almost constantly active, i.e. the solar sail acceleration lies on the cone's surface. Finally, in Fig. 16(d) the solar sail acceleration magnitude is provided, which shows an expected increase when the distance from the Sun towards Venus becomes smaller.

B. Earth NH to Venus VL Case

The optimal results for the Earth L_1 northern Halo to Venus L_2 vertical Lyapunov orbit transfer are presented in a similar way as for the Lyapunov to DPO transfer in the previous section: Tab. 5 provides departure and arrival dates and time of flights for the initial guess, the fully controllable solar sail and for different values for $\Delta\alpha$. It also contains the cone and clock angles of the optimal reference attitude of the solar sail, α_{ref} and δ_{ref}.

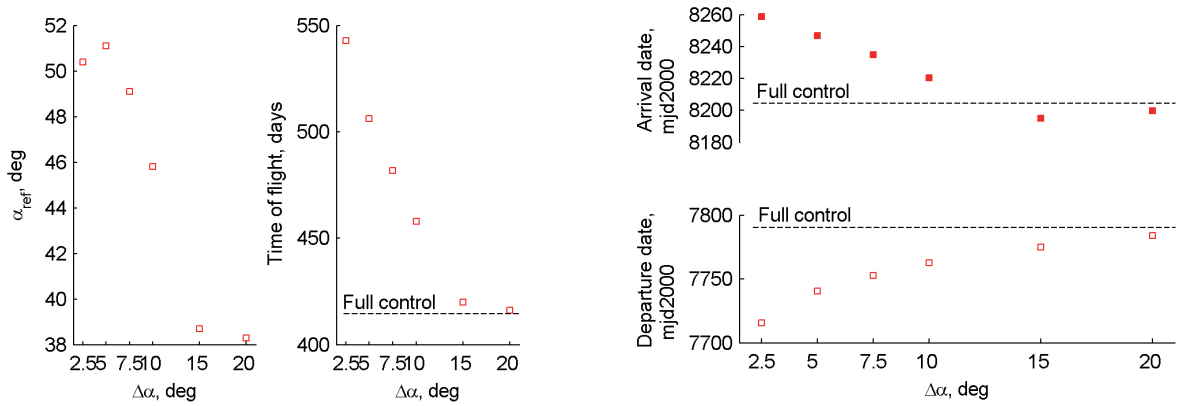

(a) Optimal sail reference attitude and time of flight.

(b) Departure and arrival times.

Figure 17. Earth L_1 northern Halo to Venus L_2 vertical Lyapunov transfers: influence of solar sail controllability, $\Delta\alpha$.

Fig. 17 provides similar information in graphical form, while Fig. 18 shows details of the transfer with $\Delta\alpha = 2.5\,\text{deg}$. Very similar conclusions as for the planar Lyapunov orbit to DRO transfer can be drawn for the northern Halo to vertical Lyapunov orbit transfer: $\Delta\alpha$ can be as small as 2.5 deg and, the smaller the value for $\Delta\alpha$, the larger the time of flight and the larger the value for α_{ref}, but the smaller the value for δ_{ref}. The latter is to ensure enough out-of-plane steering capabilities. Finally, also the penalty on the time of flight for decreasing $\Delta\alpha$ is very similar: for a fully controllable solar sail, the transfer time is 414 days which increases by 31 percent to 543 days for $\Delta\alpha = 2.5\,\text{deg}$.

VIII. Conclusions

In this paper, the first-guess generation process - based on a few design variables - of solar sail trajectories for two different applicative scenarios was investigated. In detail, LPOs belonging to the Sun–Earth system are linked to LPOs and DPOs of the Sun–Venus one, respectively. Special *dedicated sets* were introduced to exploit the combined use of solar radiation pressure with invariant manifold trajectories. This approach enabled a radically new class of missions; the key idea was to replace invariant manifolds with *solar sail sets*, and to manipulate the latter in the same way the manifolds are used to design space transfers.

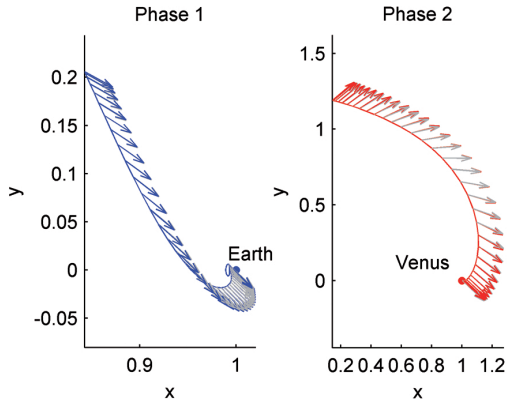

(a) Transfer phases with sail acceleration direction (color) and $\hat{\mathbf{u}}_{\text{ref}}$-direction (grey).

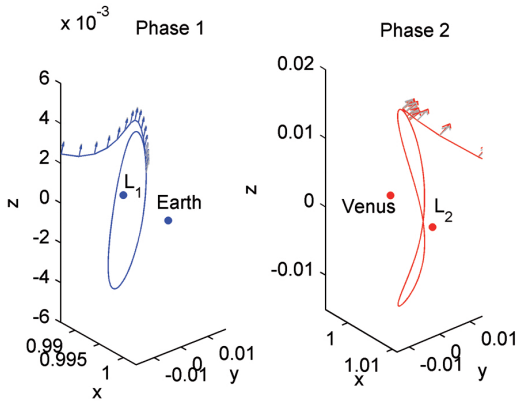

(b) Departure and arrival transfer sections.

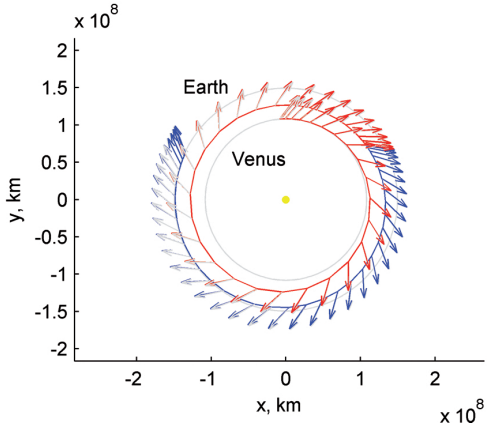

(c) Transfer in Sun-centered inertial reference frame.

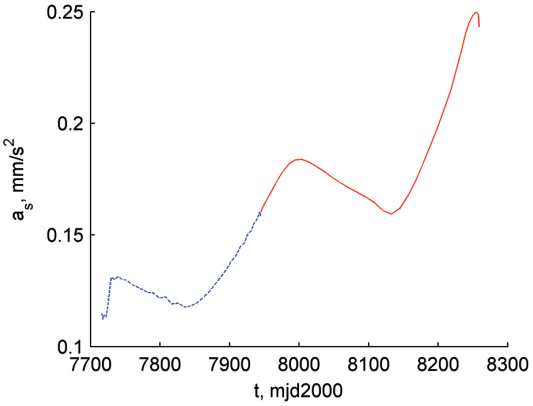

(d) Solar sail acceleration magnitude.

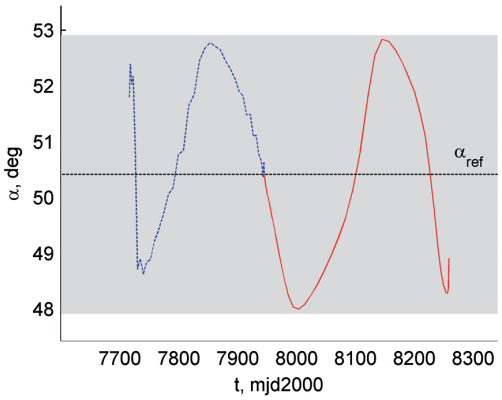

(e) Cone angle.

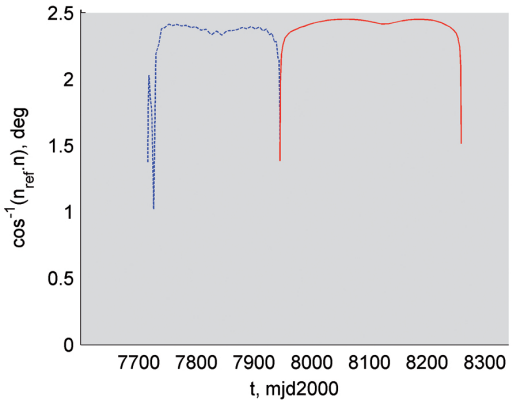

(f) Angle between $\hat{\mathbf{u}}$ and $\hat{\mathbf{u}}_{\text{ref}}$.

Figure 18. Earth L_1 northern Halo to Venus L_2 vertical Lyapunov transfer: details for $\Delta\alpha =$ 2.5 deg.

By including a solar sail acceleration and fixing the attitude of the solar sail with respect to the Sun-sail line, intersections between restricted three-body models were found on suitable Poincaré surface of sections. Alongside the exploitation of the n-body problems' intrinsic dynamics, the propellant-free feature of solar sails was used in order to generate efficient trajectories. Then an optimal control problem is formulated. The objective has been to minimise the time of flight. To that end, the optimal control problem has been derived and solved with a particular implementation of a direct pseudospectral method, PSOPT. A two-phase approach has been adopted in order to model the start of the transfer in one CRTBP and the end of the transfer in another CRTBP (including fourth-body perturbations). These phases are linked in terms of state, control and time in inertial space considering circular, ecliptic ephemerides for the planets involved. The case of low-control authority solar sails is modeled by defining a cone of half-angle $\Delta\alpha$ around a to-be optimised sail reference attitude. The results show that, for a sail performance comparable to that of NASA's Sunjammer sail, the Earth–Venus transfers can be performed with very little steering effort as $\Delta\alpha$ can be as small as 2.5 deg. Compared to a fully controllable solar sail, the penalty on the time of flight is approximately 32 percent: for the Lyapunov - DPO scenario, the transfer times are 412 days (full control) and 545 days ($\Delta\alpha = 2.5$ deg), while for the Halo - vertical Lyapunov scenario, the transfer times are 415 days (full control) and 543 days ($\Delta\alpha = 2.5$ deg), all within a 2020–2025 launch window and 2020–2027 arrival window.

IX. Acknowledgement

This research was performed in the framework of the project supported by the European Research Council Advanced Investigator Grant – 227571: VISIONSPACE, Orbital Dynamics at Extremes of Spacecraft Length-Scale.

References

[1]Tsuda, Y., Mori, O., Funase, R., Sawada, H., Yamamoto, T., Saiki, T., Endo, T., and Kawaguchi, J., "Flight Status of IKAROS Deep Space Solar Sail Demonstrator," *Acta Astronautica*, Vol. 69, 2011, pp. 833–840.

[2]Johnson, L., Whorton, M., Heaton, A., Pinson, R., Laue, G., and Adams, C., "A Solar Sail Demonstration Mission," *Acta Astronautica*, Vol. 68, 2011, pp. 571–575.

[3]McInnes, C. and Simmons, J., "Solar Sail Halo Orbits. Part I - Heliocentric Case," *Journal of Spacecraft and Rockets*, Vol. 29, 1992, pp. 466–471.

[4]Baoyin, H. and McInnes, C., "Solar Sail Halo Orbits at the Sun-Earth Artificial L1-Point," *Celestial Mechanics and Dynamical Astronomy*, Vol. 94, 2006, pp. 155–171.

[5]Pergola, P., Geurts, K., Casaregola, C., and Andrenucci, M., "Earth–Mars Halo to Halo Low Thrust Manifold Transfers," *Celestial Mechanics and Dynamical Astronomy*, Vol. 105, 2009, pp. 19–32.

[6]Topputo, F., Vasile, M., and Bernelli-Zazzera, F., "Low Energy Interplanetary Transfers Exploiting Invariant Manifolds of the Restricted Three-Body Problem," *Journal of the Astronautical Sciences*, Vol. 53, 2005, pp. 353–372.

[7]Mingotti, G. and Gurfil, P., "Mixed Low-Thrust Invariant-Manifold Transfers to Distant Prograde Orbits Around Mars," *Journal of Guidance, Control, and Dynamics*, Vol. 33, 2010, pp. 1753–1764.

[8]Mingotti, G., Topputo, F., and Bernelli-Zazzera, F., "Earth-Mars Transfers with Ballistic Escape and Low-Thrust Capture," *Celestial Mechanics and Dynamical Astronomy*, Vol. 110, 2011, pp. 169–188.

[9]Szebehely, V., *Theory of Orbits: The Restricted Problem of Three Bodies*, Academic Press Inc., New York, 1967.

[10]Conley, C., "Low Energy Transit Orbits in the Restricted Three-Body Problem," *SIAM Journal on Applied Mathematics*, Vol. 16, 1968, pp. 732–746.

[11]Llibre, J., Martínez, R., and Simó, C., "Transversality of the Invariant Manifolds Associated to the Lyapunov Family of Periodic Orbits Near L_2 in the Restricted Three-Body Problem," *Journal of Differential Equations*, Vol. 58, 1985, pp. 104–156.

[12]Gómez, G., Jorba, A., Masdemont, J., and Simó, C., "Study of the Transfer from the Earth to a Halo Orbit around the Equilibrium Point L1," *Celestial Mechanics and Dynamical Astronomy*, Vol. 56, 1993, pp. 239–259.

[13]Jorba, A. and Masdemont, J., "Dynamics in the Center Manifold of the Collinear Points of the Restricted Three Body Problem," *Physica D*, Vol. 132, 1999, pp. 189–213.

[14]Richardson, D., "Halo-orbit Formulation for the ISEE-3 Mission," *American Institute of Aeronautics and Astronautics Conference*, 1979.

[15]Richardson, D., "Analytic construction of periodic orbits about the collinear points," *Celestial Mechanics and Dynamical Astronomy*, Vol. 22, No. 3, 1980, pp. 241–253.

[16]Zagouras, C. and Markellos, V., "Three-Dimensional Periodic Solutions around Equilibrium Points in Hill's Problem," *Celestial Mechanics*, Vol. 35, No. 3, 1985, pp. 257–267.

[17]Hénon, M., "Numerical Exploration of the Restricted Problem. V," *Astron. Astrophys*, Vol. 1, 1969, pp. 223–238.

[18]Mingotti, G., Topputo, F., and Bernelli-Zazzera, F., "Transfers to Distant Periodic Orbits Around the Moon via their Invariant Manifolds," *Acta Astronautica*, Vol. 79, 2012, pp. 20–32.

[19]Koon, W., Lo, M., Marsden, J., and Ross, S., "Heteroclinic Connections between Periodic Orbits and Resonance Transitions in Celestial Mechanics," *Chaos*, Vol. 10, 2000, pp. 427–469.

[20]Wiggins, S., *Introduction to Applied Nonlinear Dynamical Systems and Chaos*, Springer Verlag, 2003.

[21]Ozimek, M. and Howell, K., "Low-Thrust Transfers in the Earth–Moon System Including Applications to Libration Point Orbits," *Journal of Guidance, Control, and Dynamics*, Vol. 33, No. 2, 2010, pp. 533–549.

[22]Ocampo, C. and Rosborough, G., "Transfer Trajectories for Distant Retrograde Orbiters of the Earth," *NASA STI/Recon Technical Report A*, Vol. 95, 1993.

[23]McInnes, C., *Solar Sailing: Technology, Dynamics and Mission Applications*, Springer-Praxis Books in Astronautical Engineering, Springer-Verlag, Berlin, 1999.

[24]Becerra, V., "Solving Complex Optimal Control Problems at No Cost with PSOPT," *Computer-Aided Control System Design (CACSD), 2010 IEEE International Symposium on*, 2010, pp. 1391–1396.

[25]Wächter, A. and Biegler, L., "On The Implementation of an Interior-Point Filter Line-Search Algorithm for Large-Scale Nonlinear Programming," *Mathematical programming*, Vol. 106, No. 1, 2006, pp. 25–57.

[26]Betts, J., "Survey of Numerical Methods for Trajectory Optimization," *Journal of Guidance, Control, and Dynamics*, Vol. 21, 1998, pp. 193–207.

[27]Bryson, A. and Ho, Y., *Applied Optimal Control*, Wiley New York, 1975.